Anthracene and pyrene appended Schiff bases having (N,N) donor for the synthesis of highly stable colloidal silver nano-particles: Application in selective sensing and nitroarene reduction

Nisha Yadav,[a] Annu Rathee,[a] Shreya Sachdeva,[a] Bharat Kumar,[b] Jahangeer Ahmed,[c] Monu Verma,[d] Gyandshwar Kumar Rao*[a]

[a]Department of Chemistry, Biochemistry and Forensic Science, Amity School of Applied Sciences, Amity University Haryana, Manesar, Gurgaon-122413, Haryana, India.
[b]Department of Chemistry, M V College Buxar, (A constituent unit of Veer Kunwar Singh University Arrah) Bihar-802101, India.
[c]Department of Chemistry, College of Science, King Saud University, P.O. Box 2455, Riyadh 11451, Saudi Arabia.
Water-Energy Nexus Laboratory, Department of Environmental Engineering, University of Seoul, Seoul, 02504, South Korea.
*gyan23iitd@gmail.com, gkrao@ggn.amity.edu

NMR Data of Ligands

L1: Yield: 0.395 g (90%); NMR: (^{1}H, 500 MHz, $CDCl_3$, 25 °C, TMS): δ (ppm): 9.52 (s, 2H); 8.49 (s, 2H); 8.44 (d, 4H, J = 10 Hz); 7.98 (d, 4H, J = 10 Hz); 7.38 (t, 4H, J = 10 Hz); 7.17-7.12 (m, 4H); 4.54 (s, 4H). ^{13}C{^{1}H}, 125 MHz, $CDCl_3$, 25 °C, TMS): δ (ppm): 159.8, 130.7, 129.6, 129.0, 128.0, 127.5, 126.1, 125.0, 124.2, 62.9. IR (cm^{-1}) **L1**: 3041, 2899, 2325, 1938, 1804, 1635, 1513, 1438, 1379, 1252, 1157, 1021, 969, 946, 879, 833, 782, 723.

L2: Yield: 0.432 g (88%); NMR: (^{1}H, 500 MHz, $CDCl_3$, 25 °C, TMS): δ (ppm): 9.45 (s, 2H); 8.51 (d, 6H, J = 10 Hz); 8.03 (d, 5H, J = 5 Hz); 7.55-7.48 (m, 9H); 4.01 (t, 4H, J = 5 Hz); 1.75-1.72 (m, 4H). ^{13}C{^{1}H}, 125 MHz, $CDCl_3$, 25 °C, TMS): δ (ppm): 160.1, 131.3, 129.9, 129.1, 128.8, 128.2, 126.6, 125.2, 124.8, 31.0, 27.4. IR (cm^{-1}) **L2**: 3041, 2929, 2840, 1915, 1774, 1631, 1513, 1341, 1386, 1446, 1304, 1252, 1058, 1155, 946, 879, 834, 782, 723.

L3: Yield: 0.459 g (87%); NMR: (^{1}H, 500 MHz, $CDCl_3$, 25 °C, TMS): δ (ppm): 9.35 (s, 2H); 8.71 (d, 2H, J= 10 Hz); 8.54 (d, 2H, J= 10 Hz); 8.33−7.87 (m, 14H); 7.81 (d, 2H J= 5 Hz); 4.38 (s, 4H). (^{13}C{^{1}H}, 125 MHz, $CDCl_3$, 25 °C, TMS): δ (ppm): 162.1, 132.8, 131.1, 130.4, 129.8, 128.7, 128.4, 128.3, 127.3, 126.1, 125.9, 125.7, 125.4, 124.8, 124.7, 124.5, 122.3, 62.4. IR (cm^{-1}) **L3**: 3041, 2907, 2840, 1908, 1781, 1677, 1625, 1595, 1535, 1505, 1483, 1453, 1431, 1408, 1386, 1319, 1282, 1237, 1177, 1088, 1051, 1013, 986, 894, 745, 715, 685.

L4: Yield: 0.445 g (82%); NMR: (^{1}H, 500 MHz, $CDCl_3$, 25 °C, TMS): δ (ppm): 9.33 (s, 2H); 8.89 (d, 2H, J = 10 Hz); 8.53 (d, 2H, J = 10 Hz); 8.24−8.01 (m, 14H); 3.90 (t, 4H, J = 5 Hz); 1.96 (t, 4H, J = 5 Hz); 1.65 (m, 4H). (^{13}C{^{1}H}, 125 MHz, $CDCl_3$, 25 °C, TMS): δ (ppm): 159.6, 132.8, 131.4, 130.7, 129.8, 129.0, 128.6, 128.5, 127.6, 126.4, 126.2, 125.9, 125.6, 125.1, 125.0, 124.8, 122.8, 62.8, 31.2, 27.4. IR (cm^{-1}) **L4**: 3034, 2922, 2847, 1915, 1781, 1677, 1625, 1595, 1431, 1386, 1356, 1304, 1237, 1177, 1095, 1021, 969, 931, 887, 849, 820, 745, 715, 685.

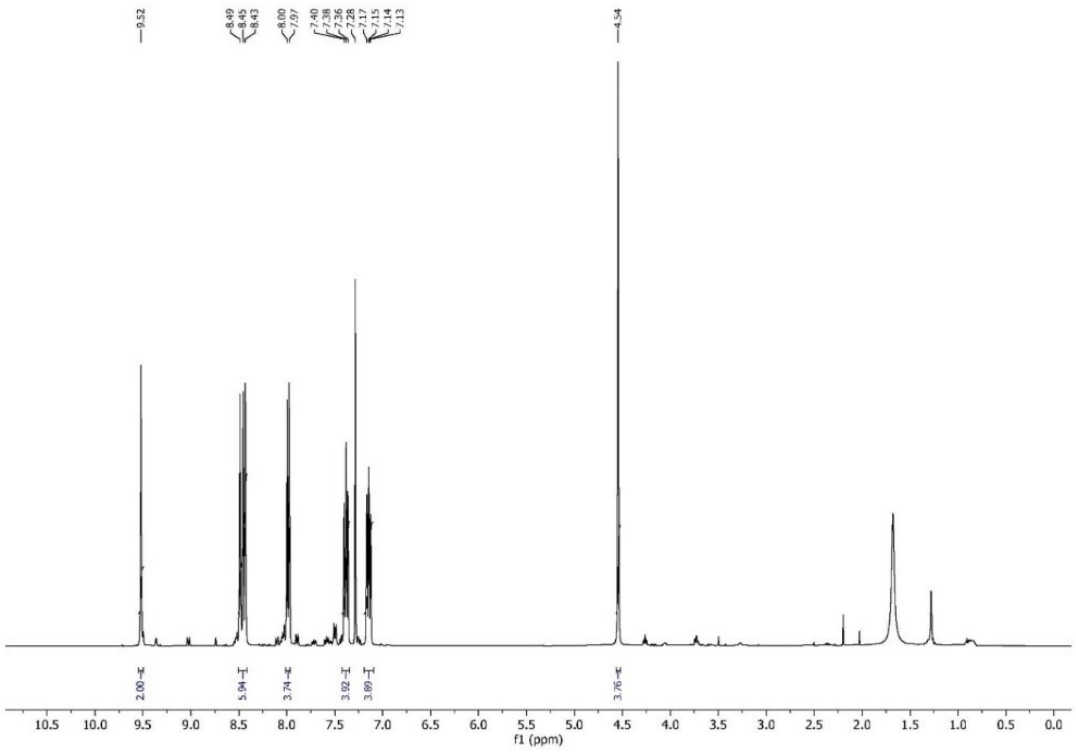

Figure S1. ^{1}H NMR spectra of **L1**

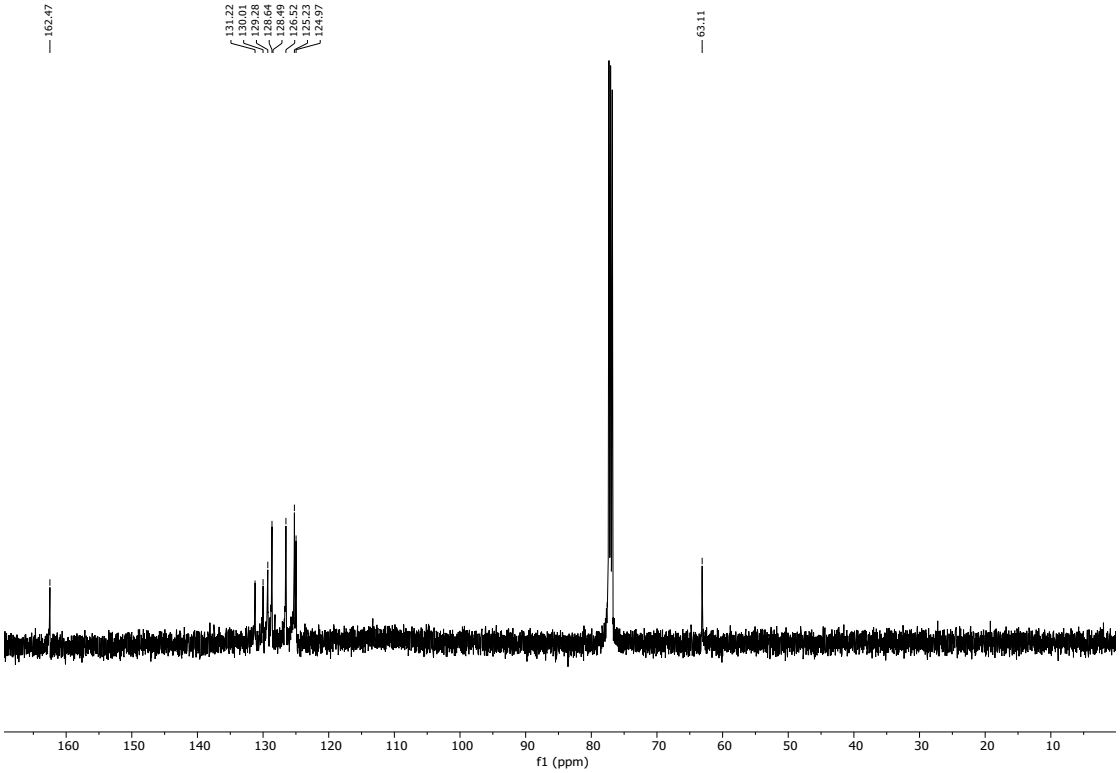

Figure S2. $^{13}C\{^{1}H\}$ NMR spectra of **L1**

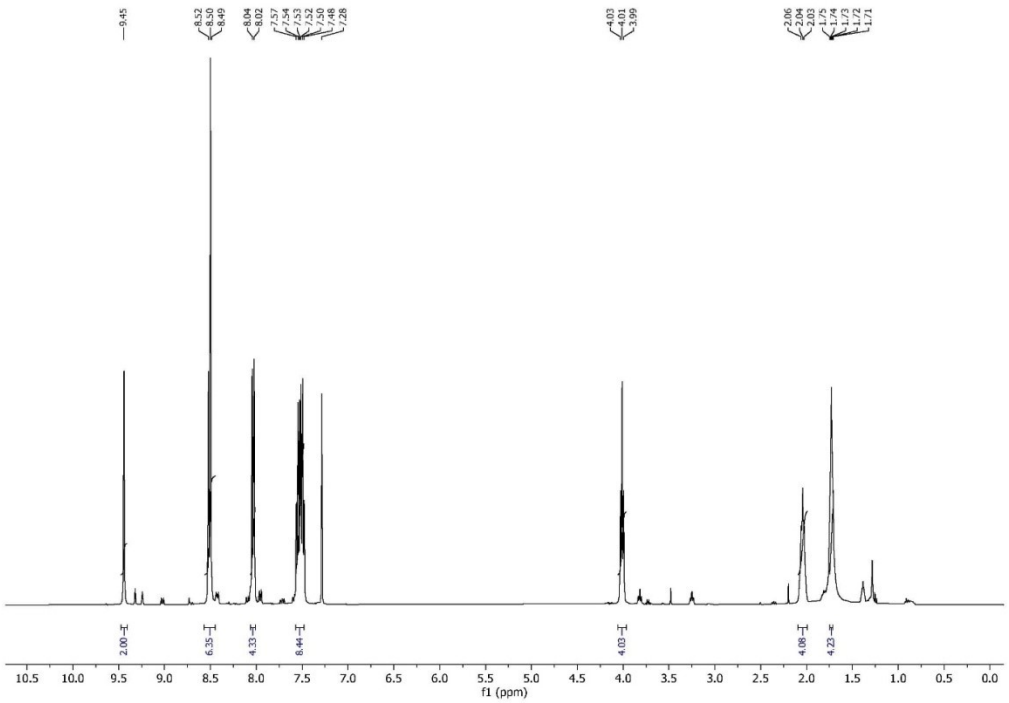

Figure S3. ^{1}H NMR spectra of **L2**

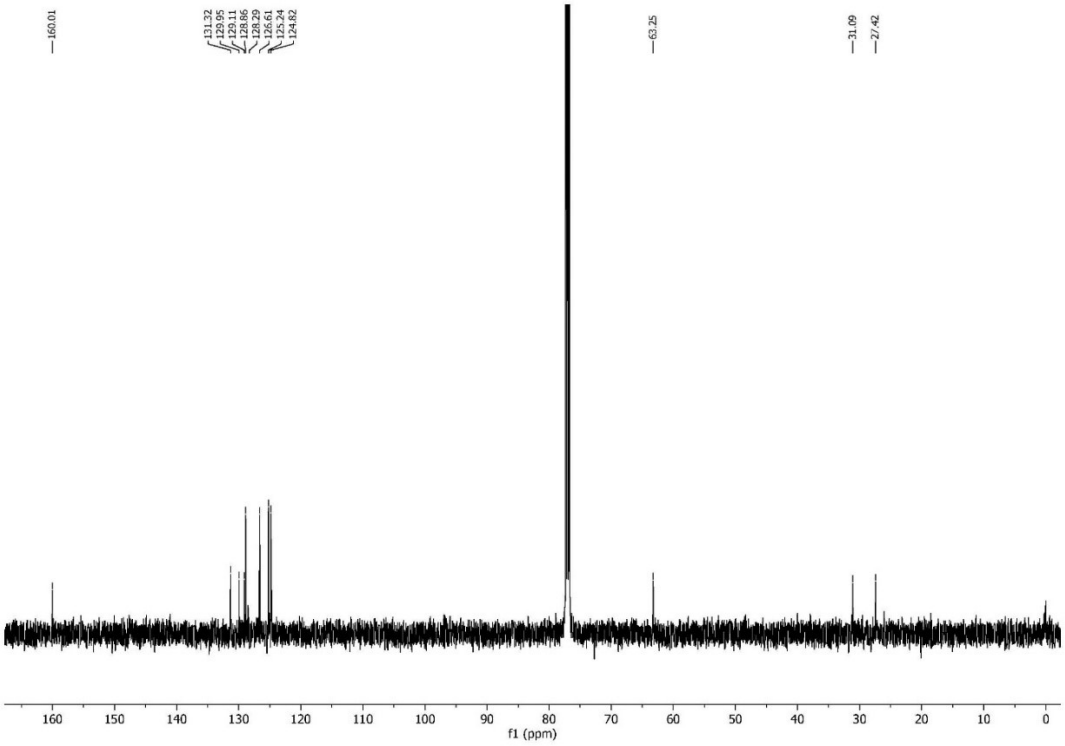

Figure S4. ^{13}C{^{1}H} NMR spectra of **L2**

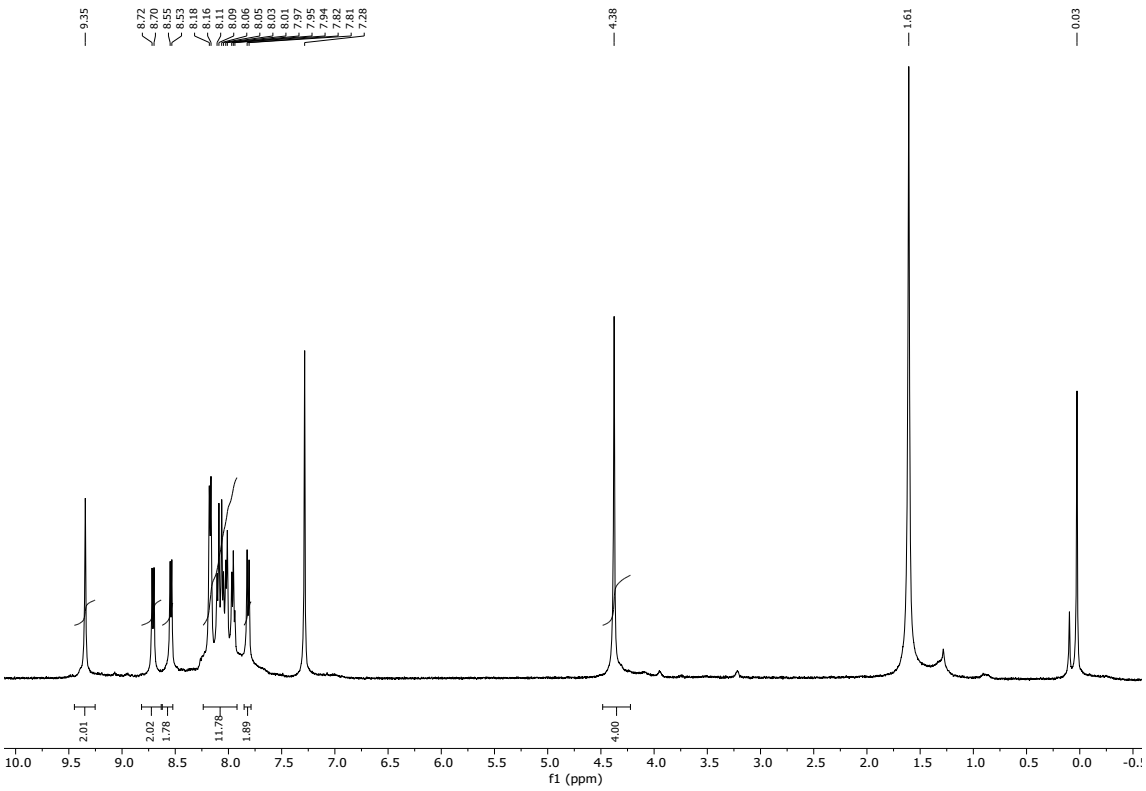

Figure S5. ^{1}H NMR spectra of **L3**

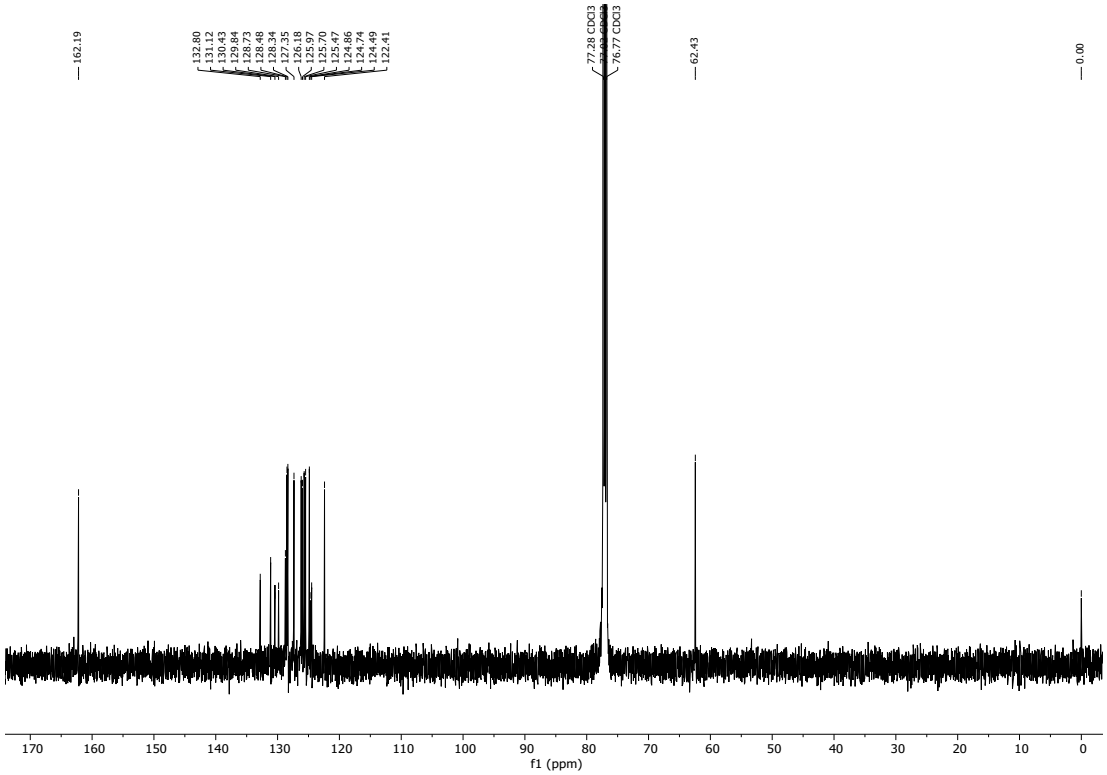

Figure S6. ^{13}C{^{1}H} NMR spectra of **L3**

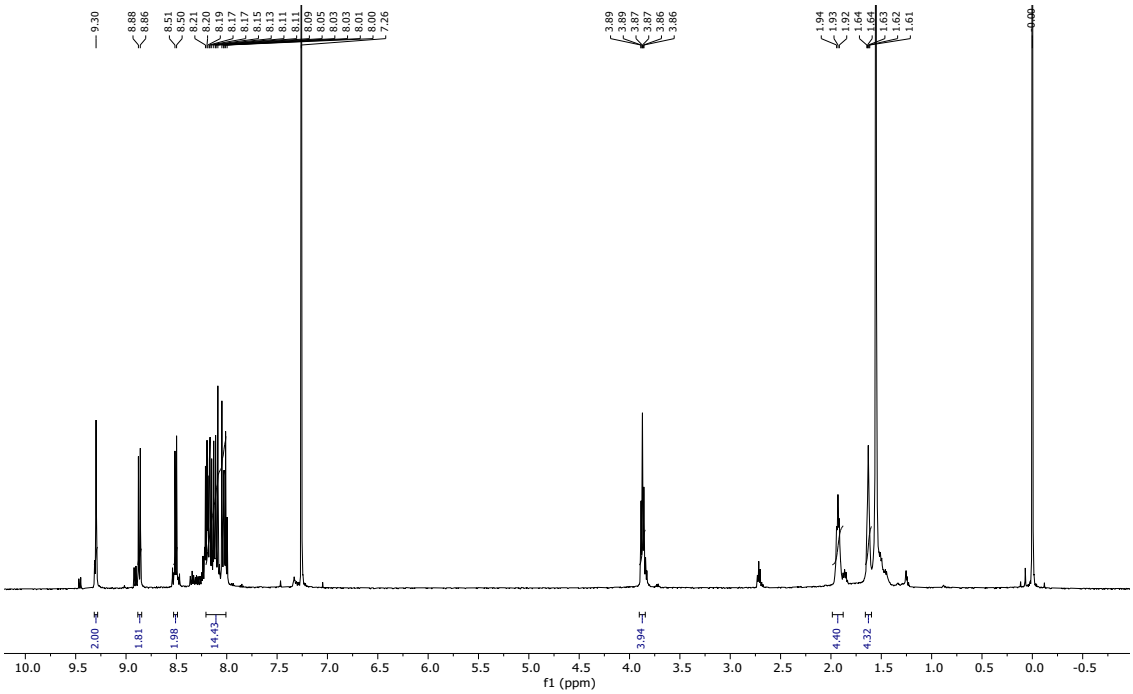

Figure S7. ^{1}H NMR spectra of **L4**

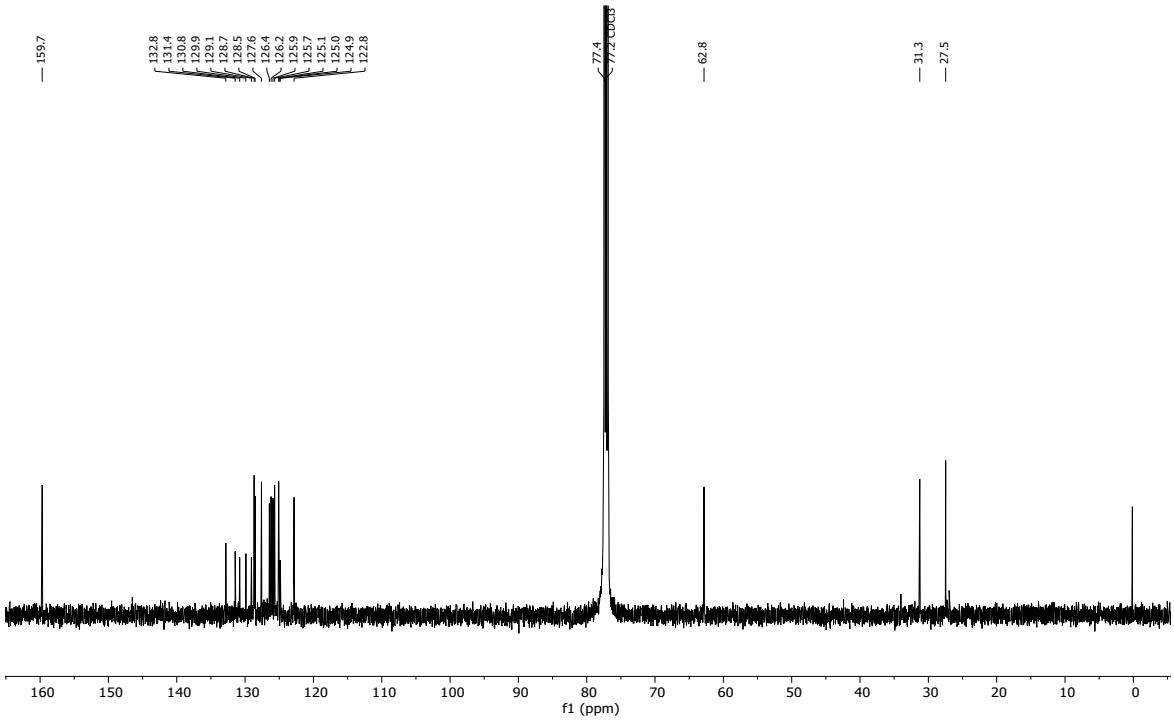

Figure S8. ^{13}C{^{1}H} NMR spectra of **L4**

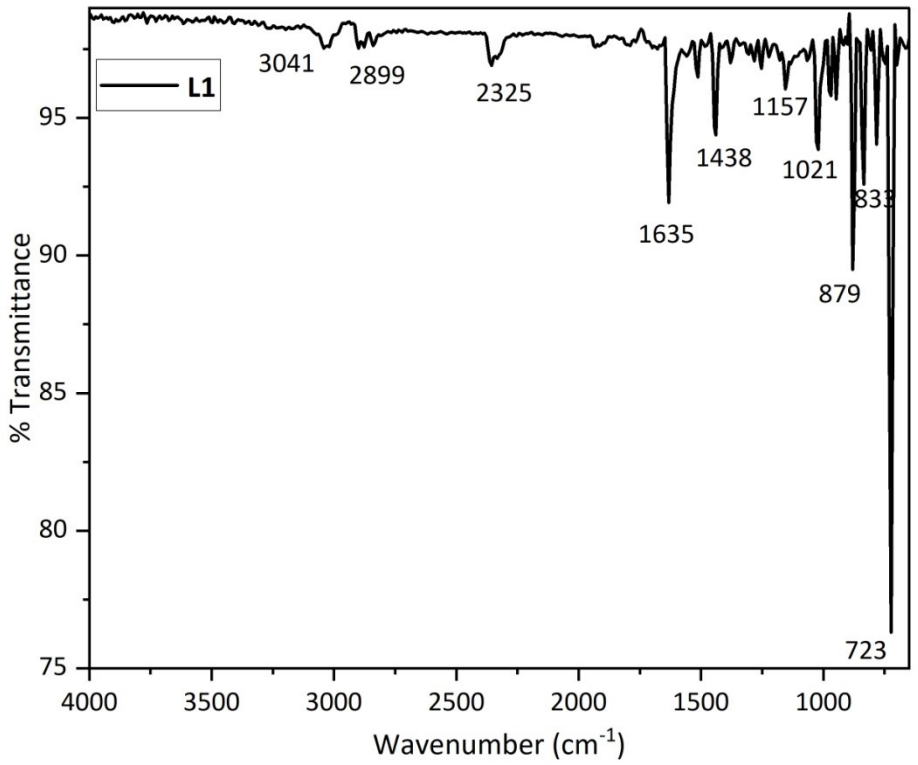

Figure S9. Infrared spectra of **L1**

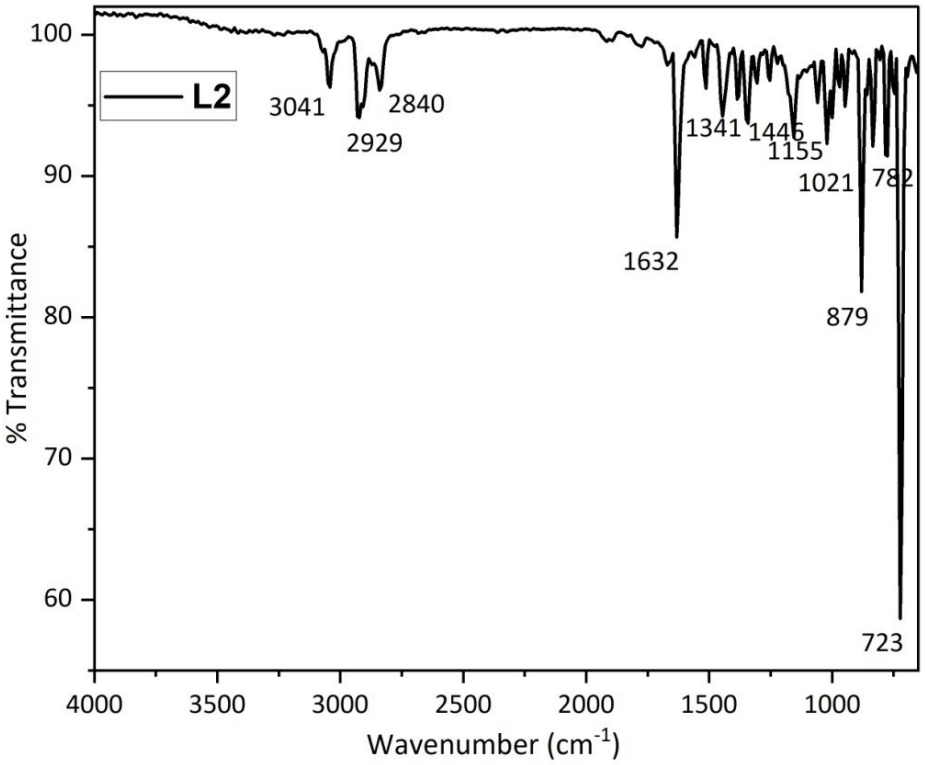

Figure S10. Infrared spectra of **L2**

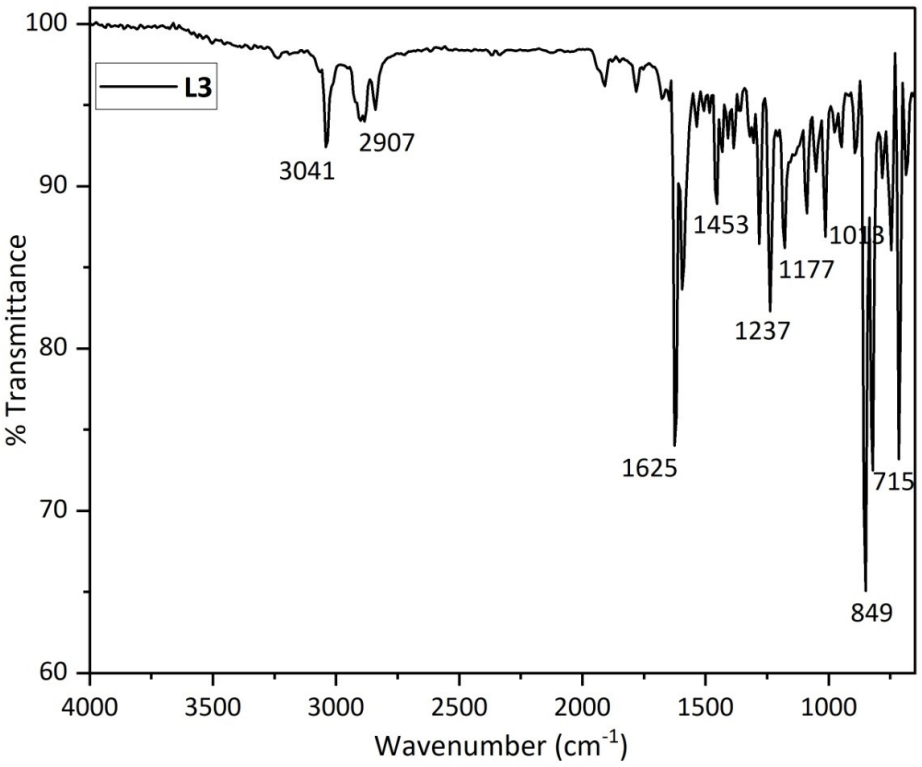

Figure S11. Infrared spectra of **L3**

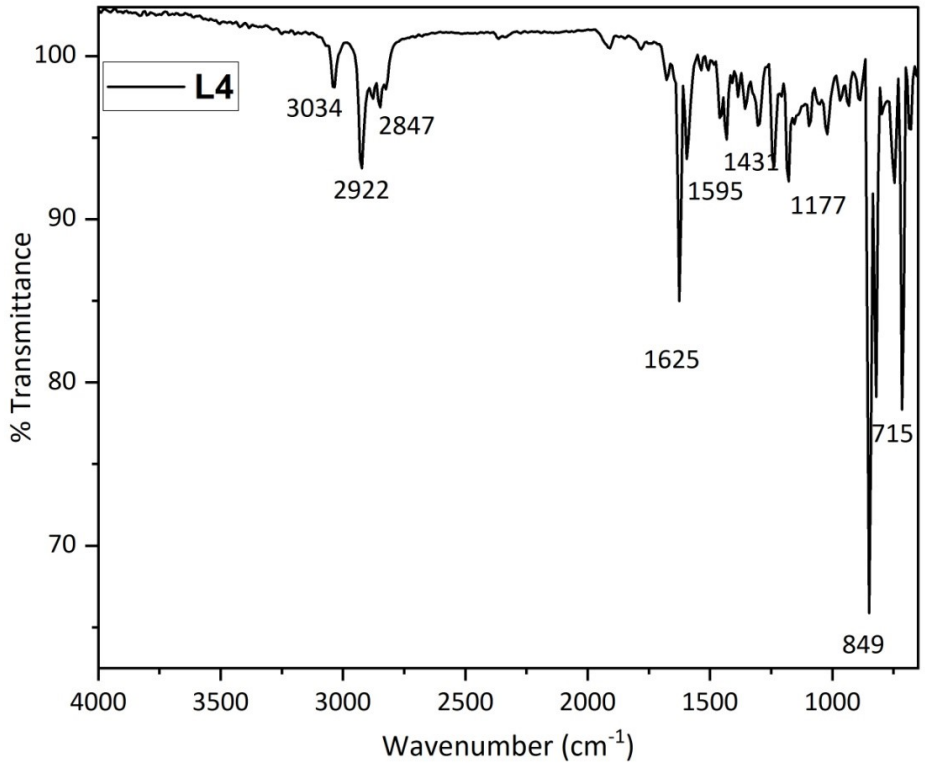

Figure S12. Infrared spectra of **L4**

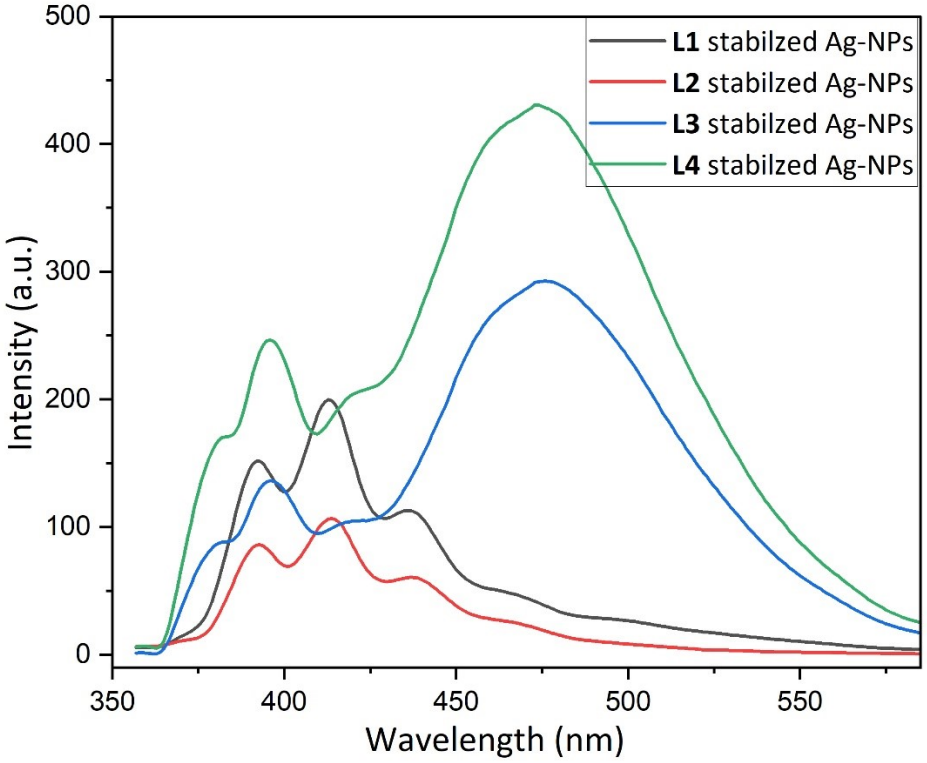

Figure S13. Fluorescence spectra of **L1−L4** stabilized silver nanoparticles

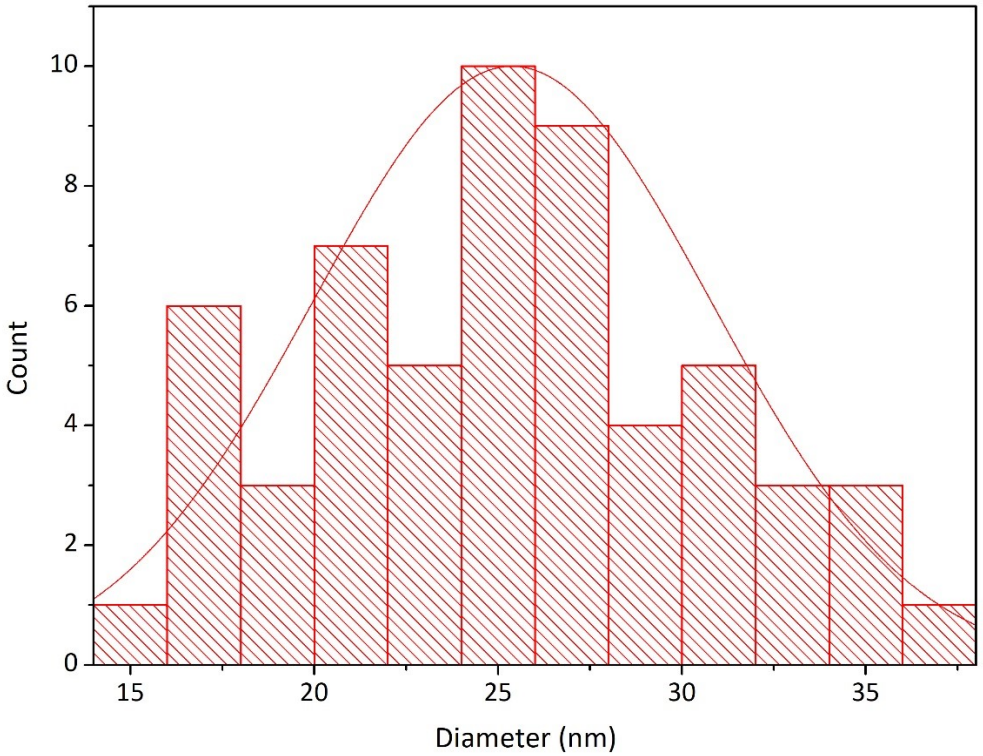

Figure S14. Particle size distribution in the case of **L1** stabilized silver nanoparticles

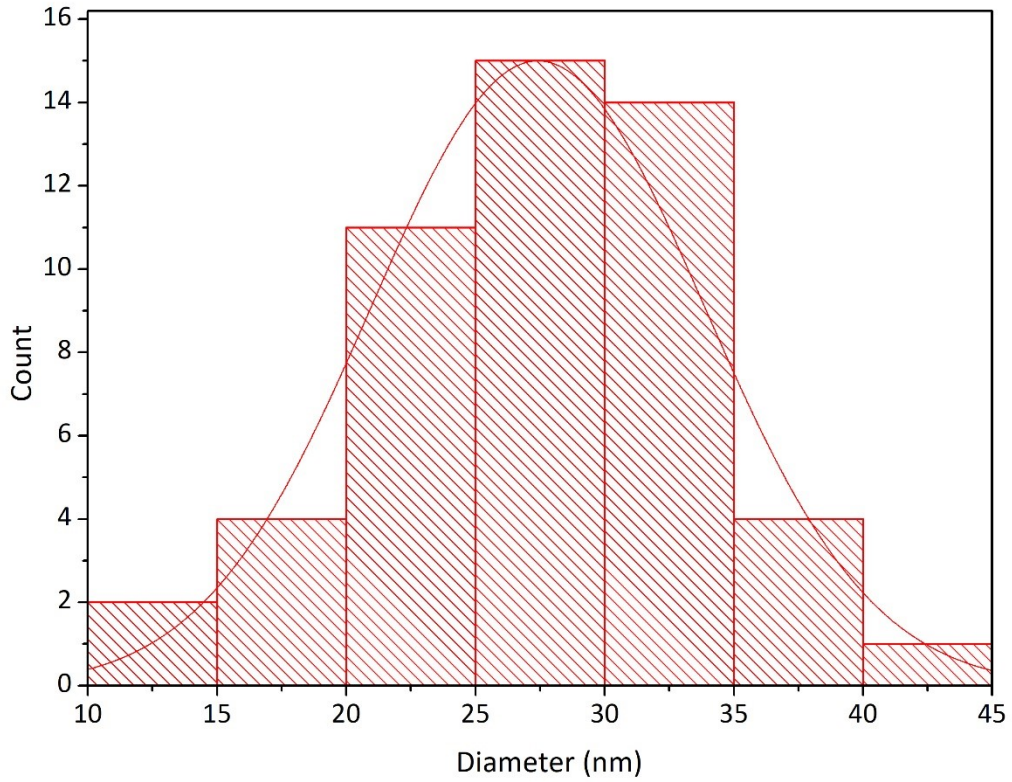

Figure S15. Particle size distribution in the case of **L2** stabilized silver nanoparticles

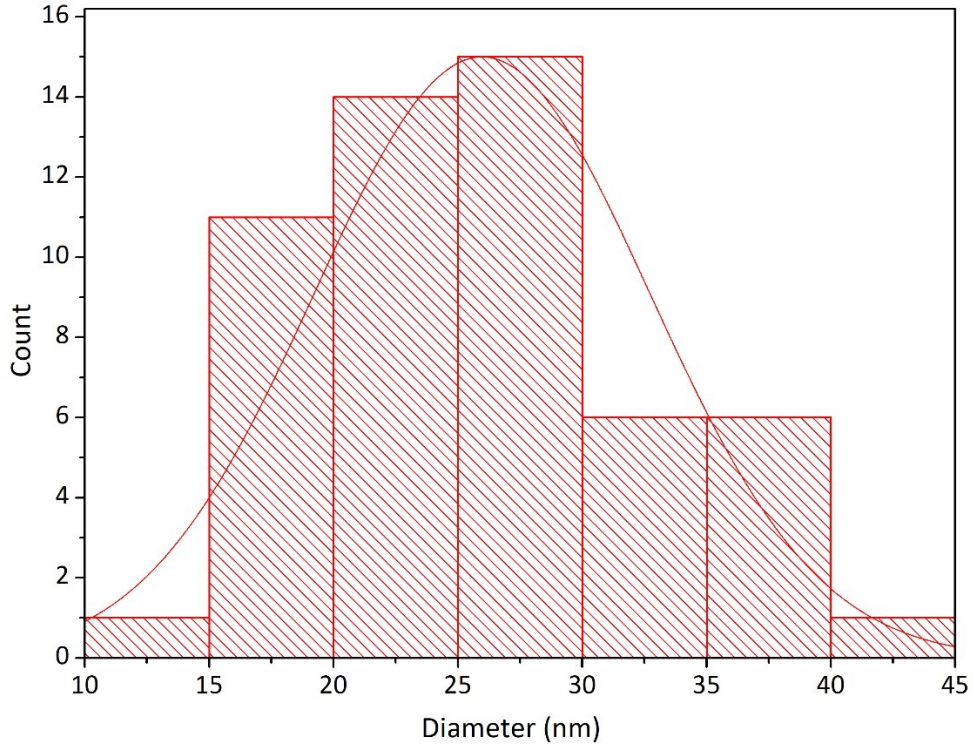

Figure S16. Particle size distribution in the case of **L3** stabilized silver nanoparticles

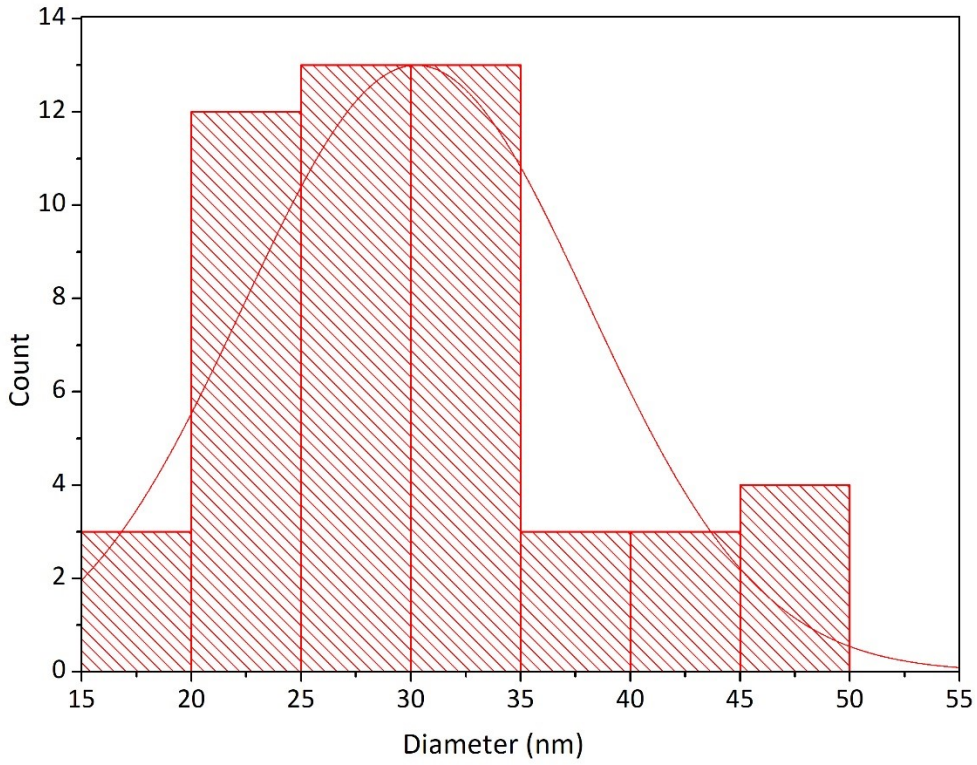

Figure S17. Particle size distribution in the case of **L4** stabilized silver nanoparticles

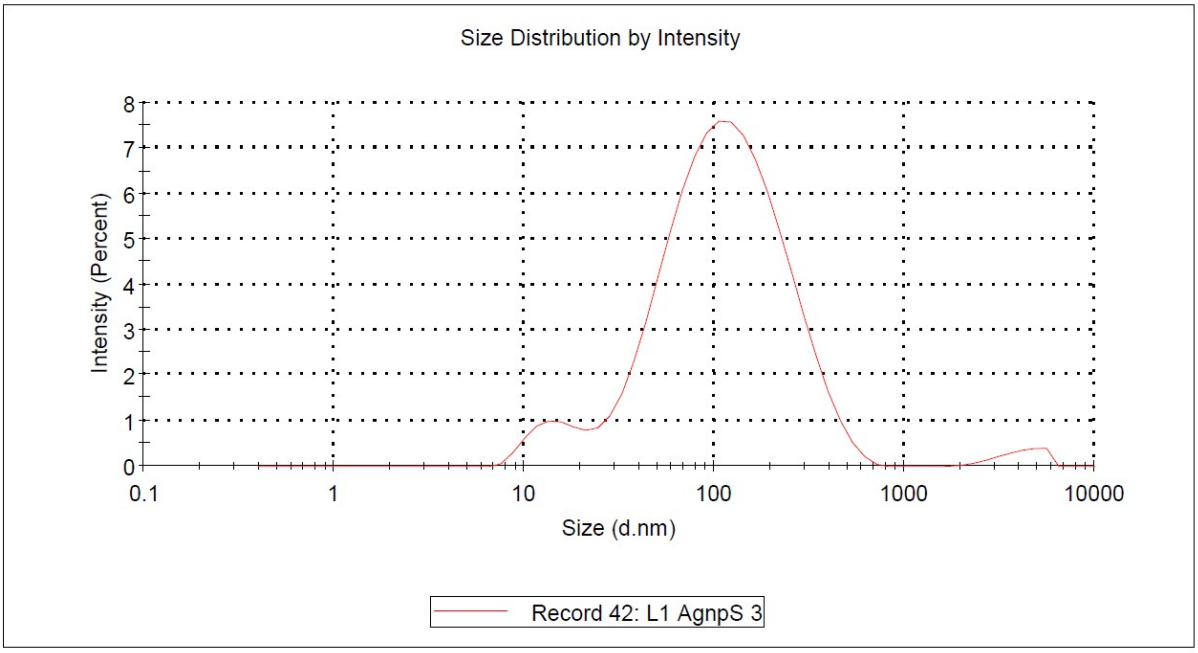

Figure S18. DLS data of **L1** stabilized silver nanoparticles (freshly synthesized)

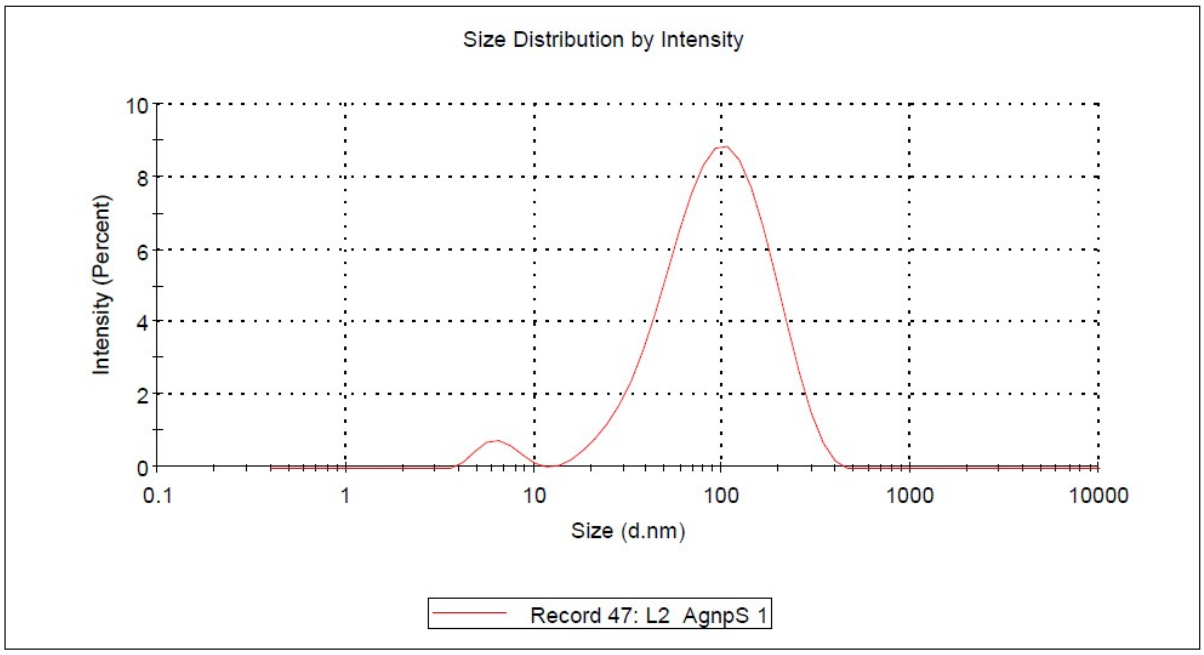

Figure S19. DLS data of **L2** stabilized silver nanoparticles (freshly synthesized)

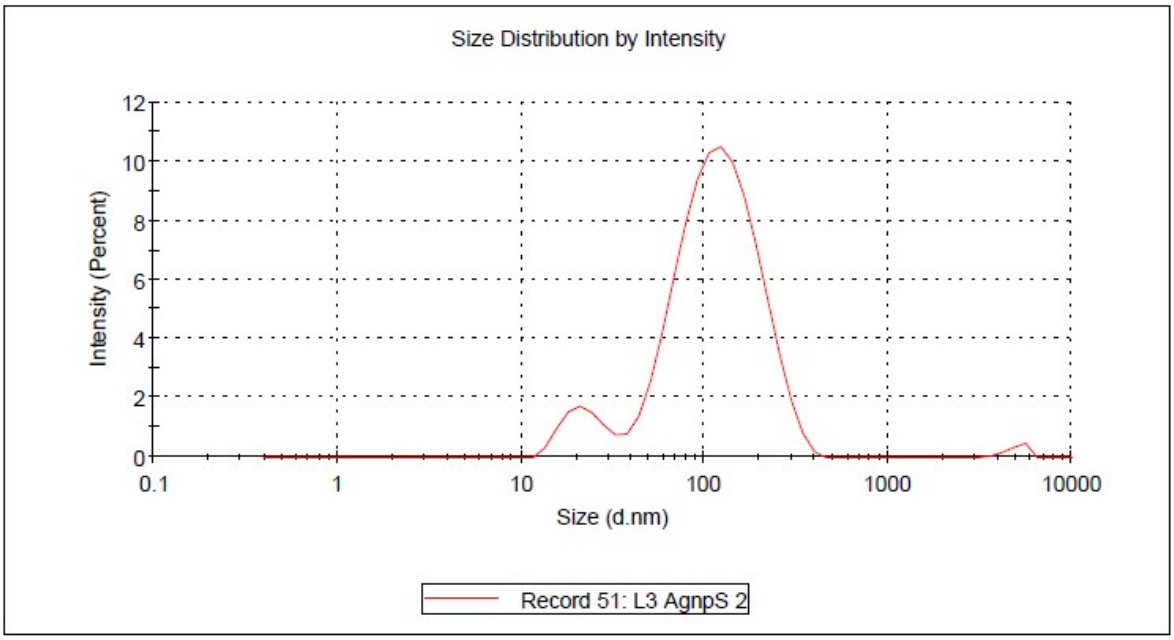

Figure S20. DLS data of **L3** stabilized silver nanoparticles (freshly synthesized)

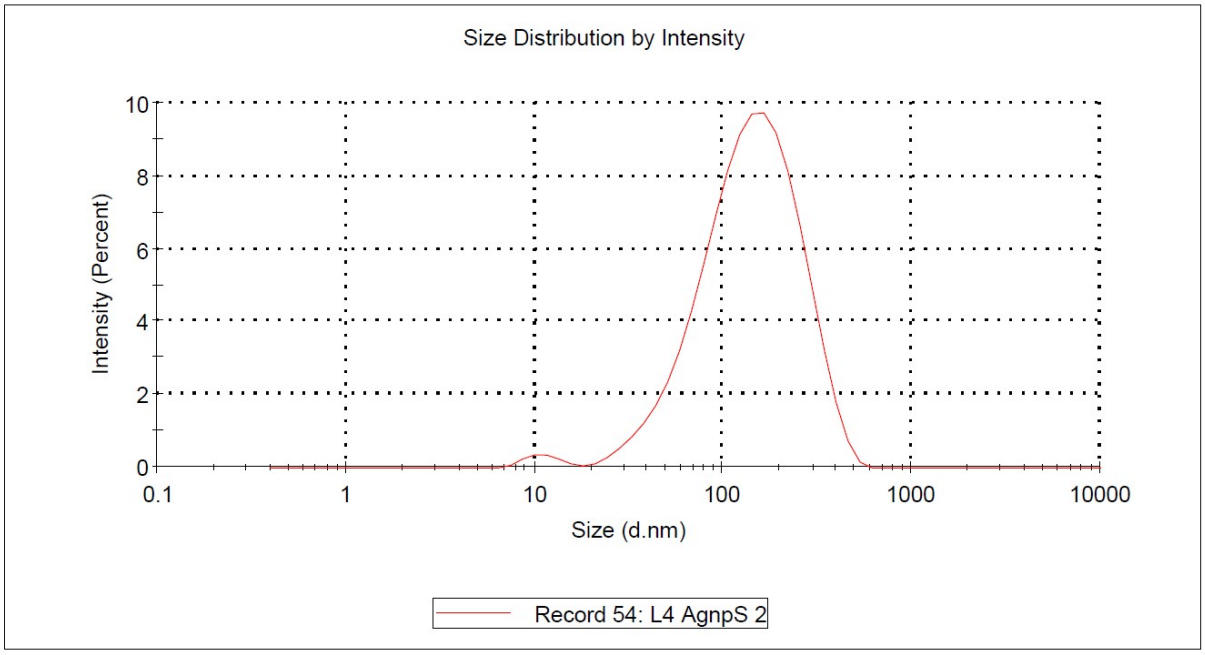

Figure S21. DLS data of **L4** stabilized silver nanoparticles (freshly synthesized)

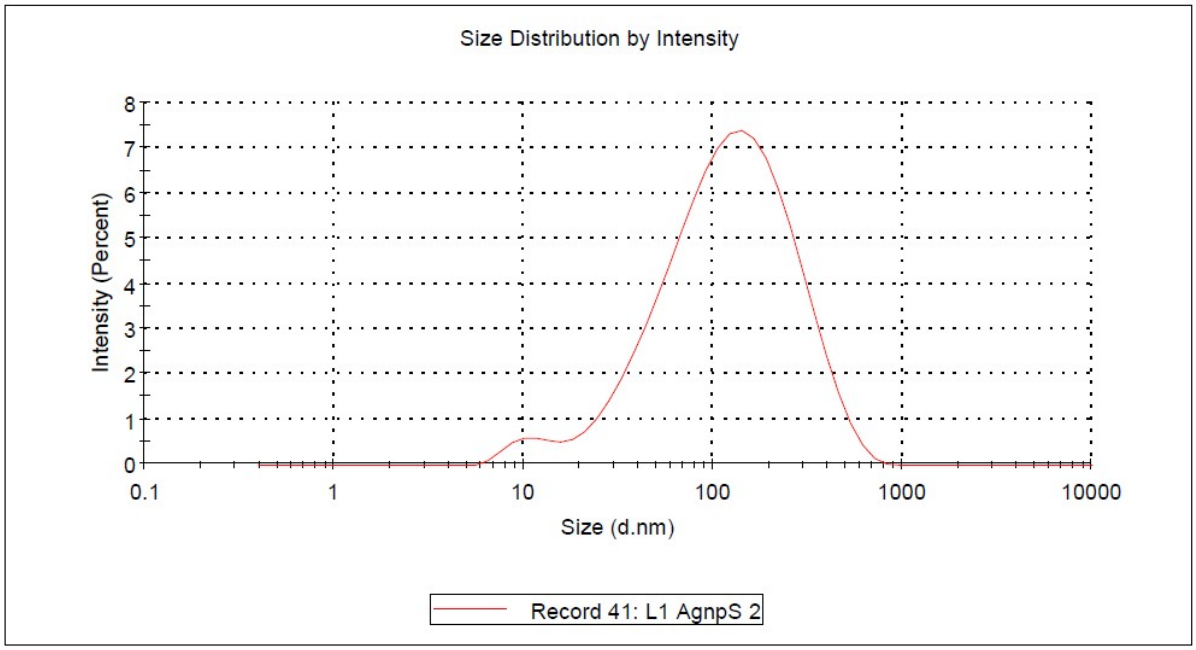

Figure S22. DLS data of **L1** stabilized silver nanoparticles (at 15th day)

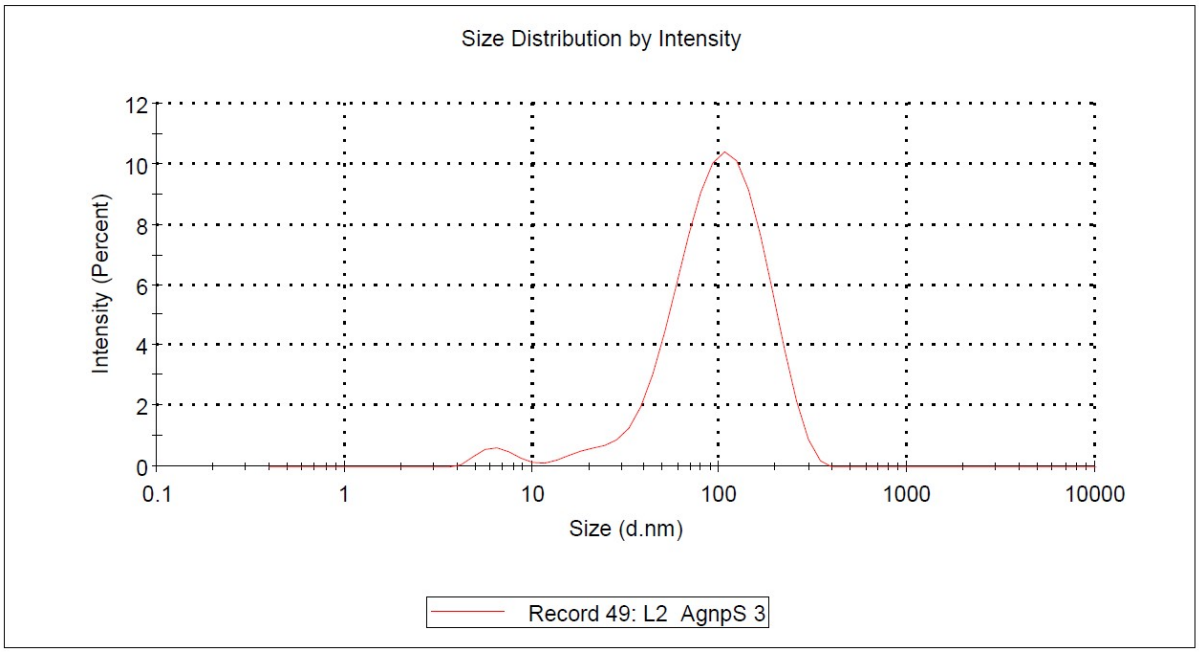

Figure S23. DLS data of **L2** stabilized silver nanoparticles (at 15th day)

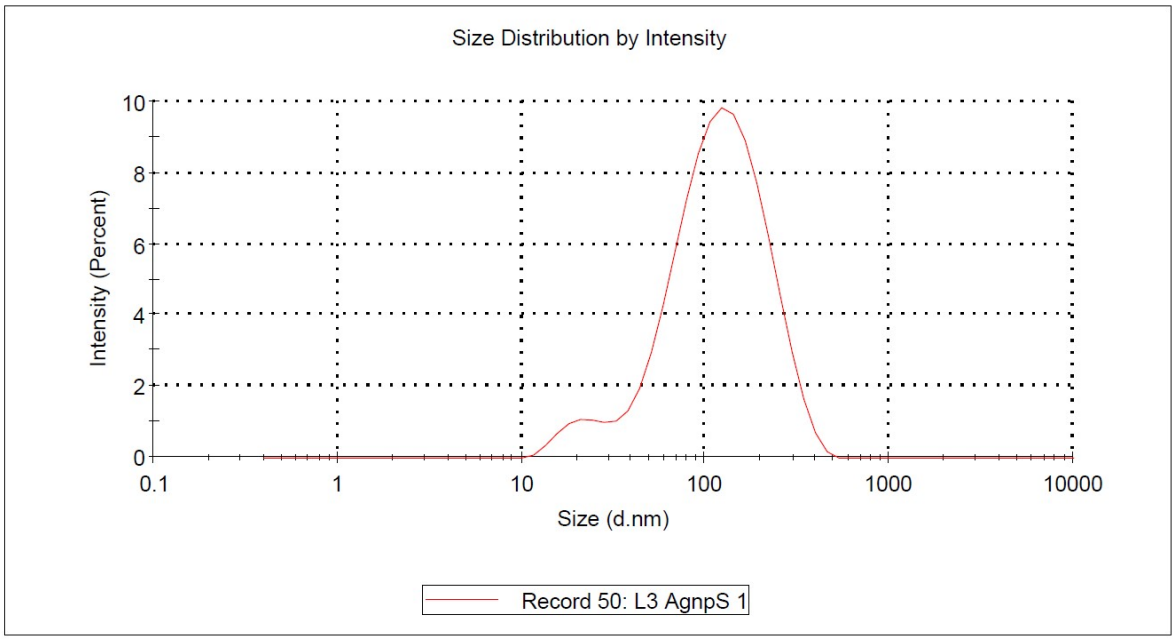

Figure S24. DLS data of **L3** stabilized silver nanoparticles (at 15th day)

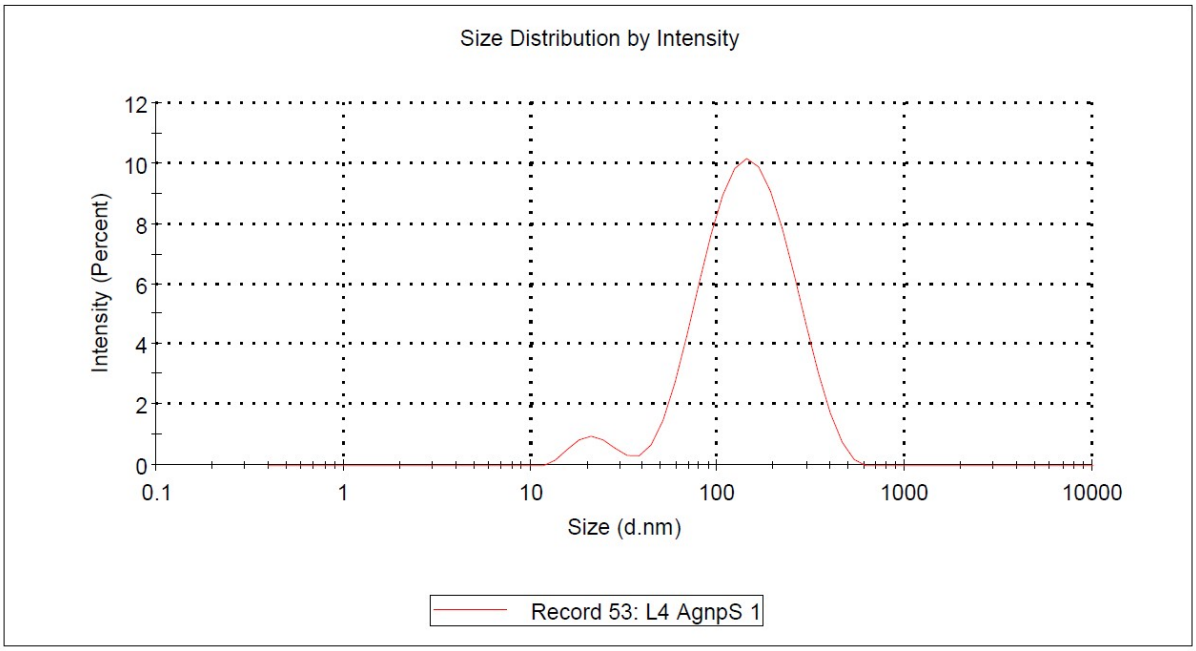

Figure S25. DLS data of **L4** stabilized silver nanoparticles (at 15th day)

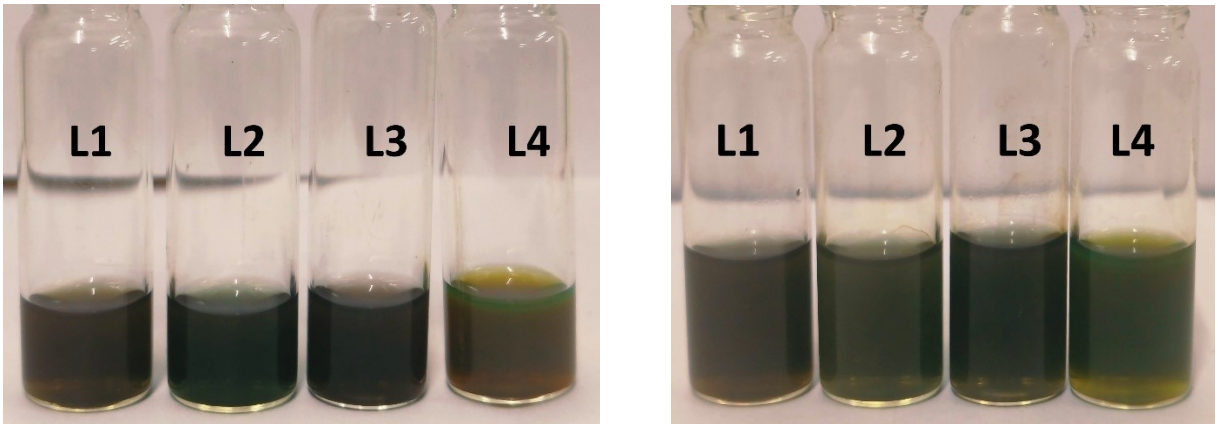

(a) **(b)**

Figure S26. Photographs of; (a) as-synthesized colloidal Ag-NPs and (b) colloidal Ag-NPs at 60th day

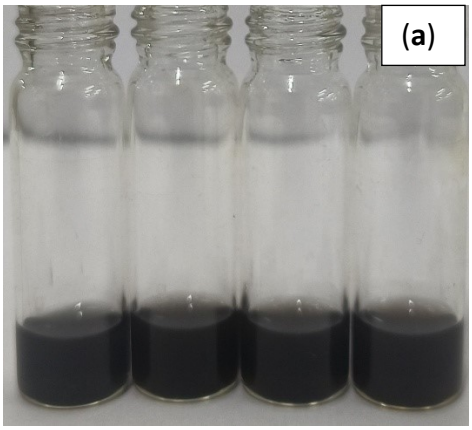

L1 Pb^{2+} As^{3+} Cd^{2+}

L1 NO_3^- SO_4^{2-}

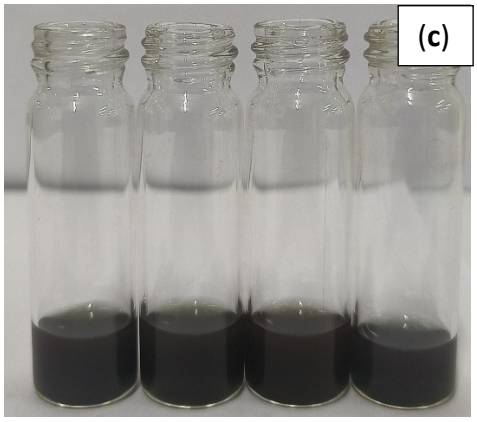

L2 Pb^{2+} As^{3+} Cd^{2+}

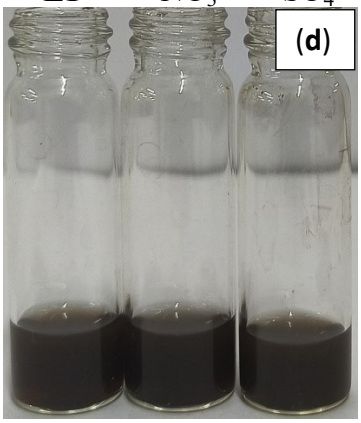

L2 NO_3^- SO_4^{2-}

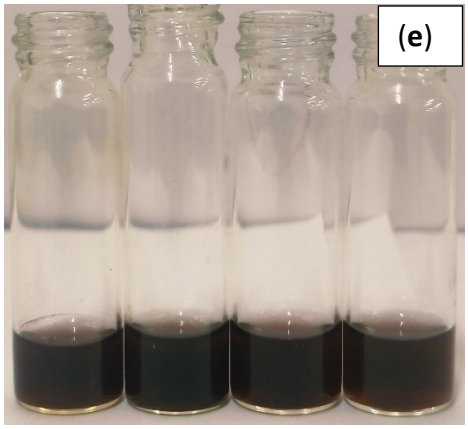

L3 Pb^{2+} As^{3+} Cd^{2+}

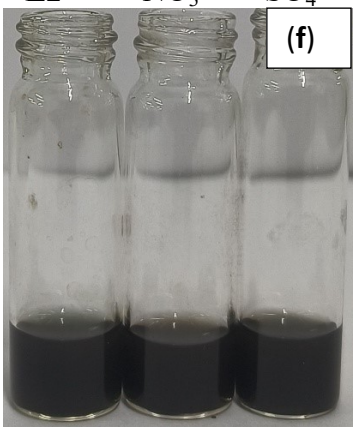

L3 NO_3^- SO_4^{2-}

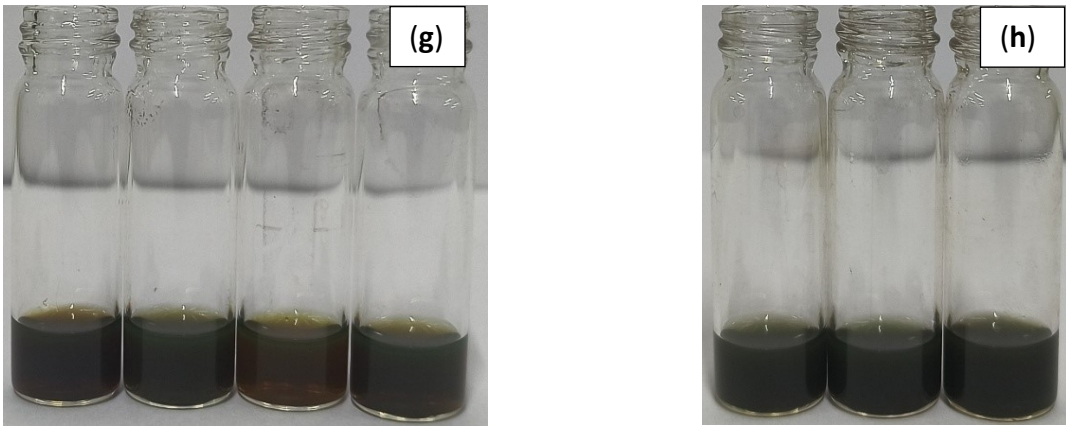

Figure S27. Colorimetric sensing of metal ions with added metal salt {Pb^{2+}, As^{3+}, Cd^{2+} (10 µL of 50 mM)} in the colloidal solution of (a) **L1** capped Ag-NPs; (c) **L2** capped Ag-NPs; (e) **L3** capped Ag-NPs; (g) **L4** capped Ag-NPs; and with added anions {NO_3^-, SO_4^-; (10 µL of 10 mM)} in the colloidal solution of (b) **L1** capped Ag-NPs; (d) **L2** capped Ag-NPs; (f) **L3** capped Ag-NPs; (h) **L4** capped Ag-NPs.

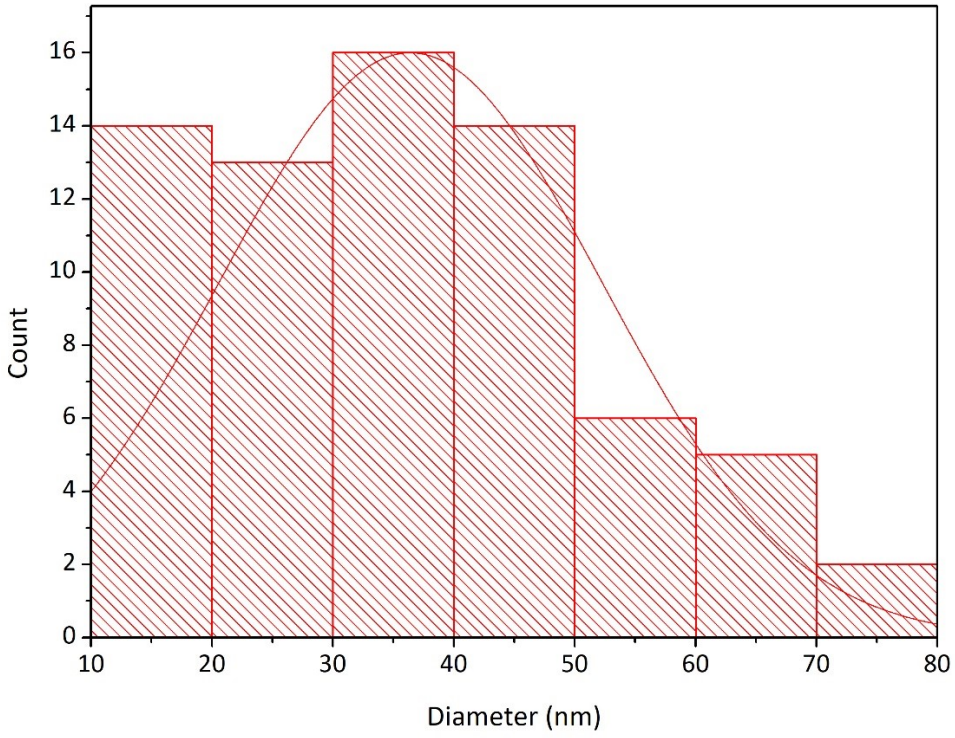

Figure S28. Particle size distribution in the case of **L1** stabilized silver nanoparticles after the addition of Hg^{2+} ions

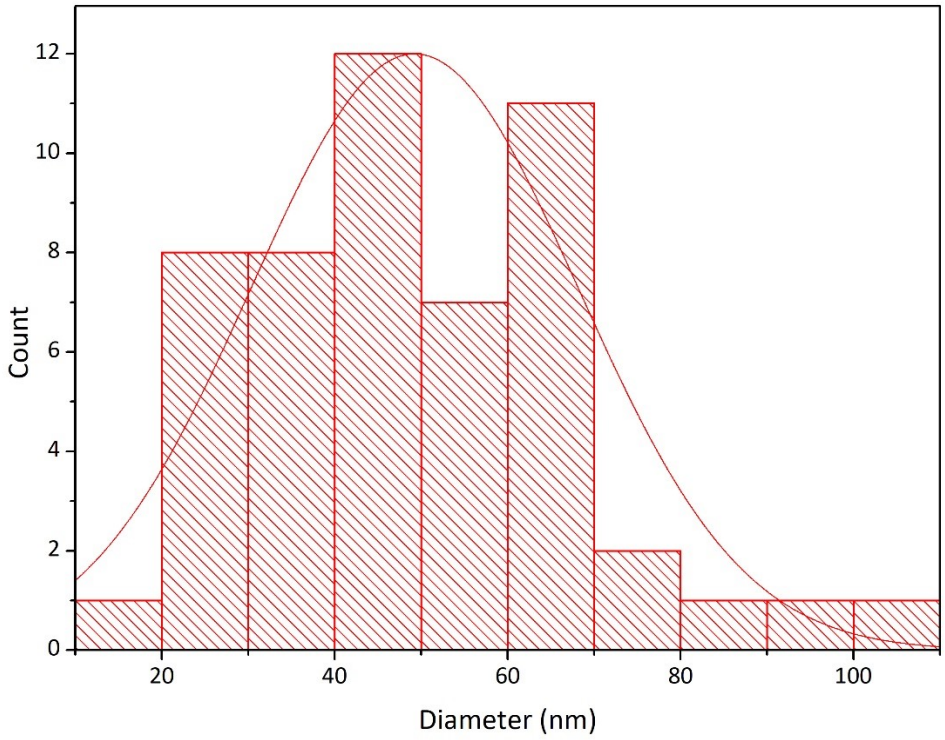

Figure S29. Particle size distribution in the case of **L1** stabilized silver nanoparticles after the addition of Cl^- ions

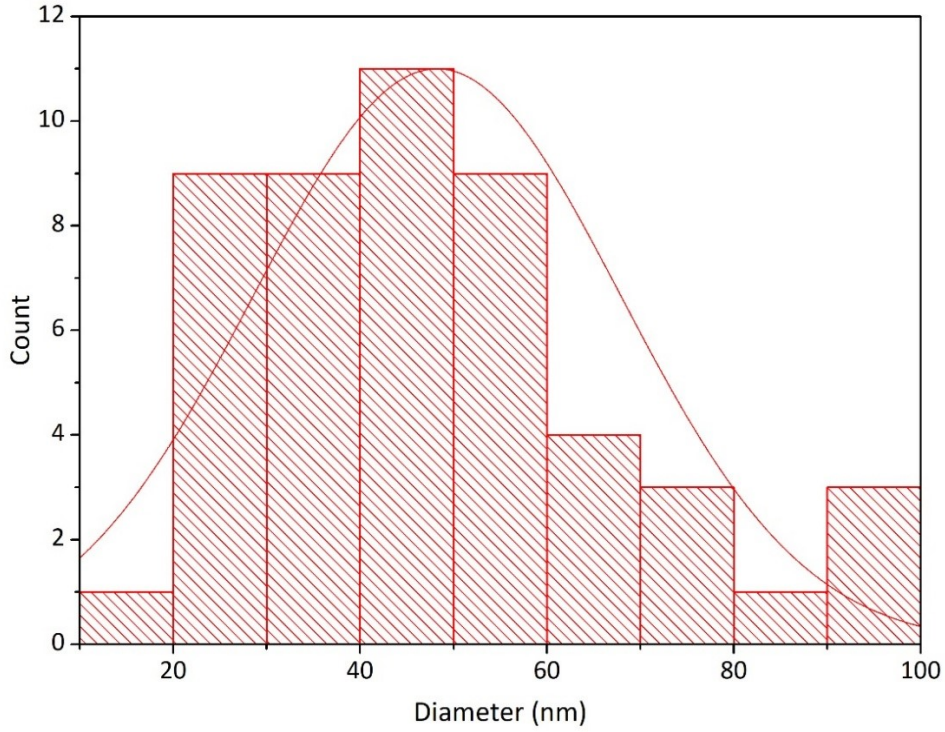

Figure S30. Particle size distribution in the case of **L2** stabilized silver nanoparticles after the addition of Hg^{2+} ions

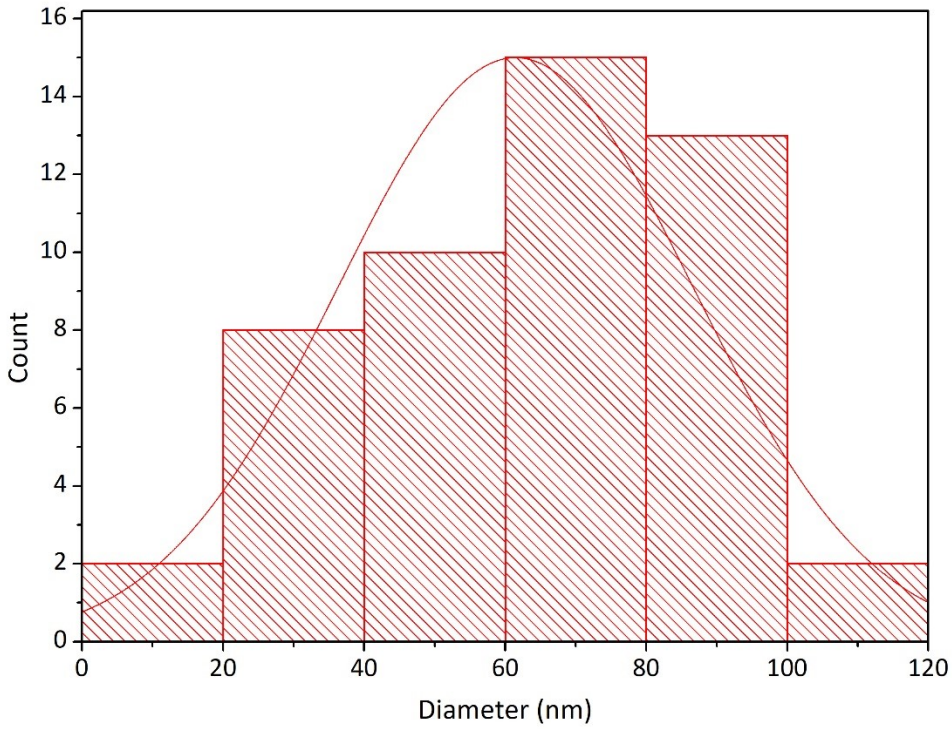

Figure S31. Particle size distribution in the case of **L2** stabilized silver nanoparticles after the addition of Bi^{3+} ions

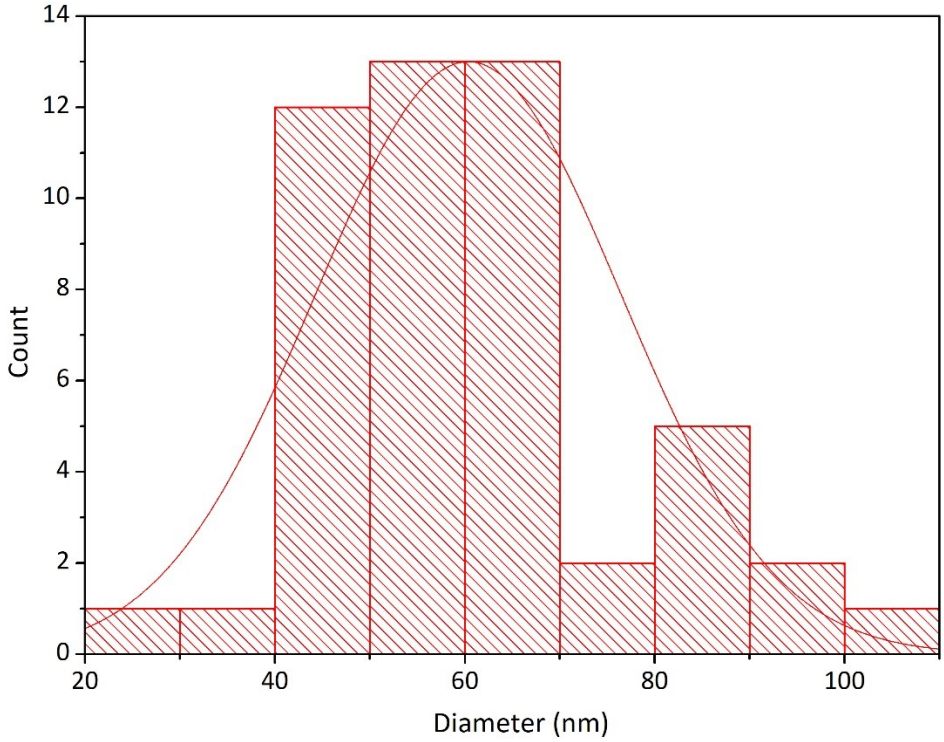

Figure S32. Particle size distribution in the case of **L2** stabilized silver nanoparticles after the addition of I^- ions

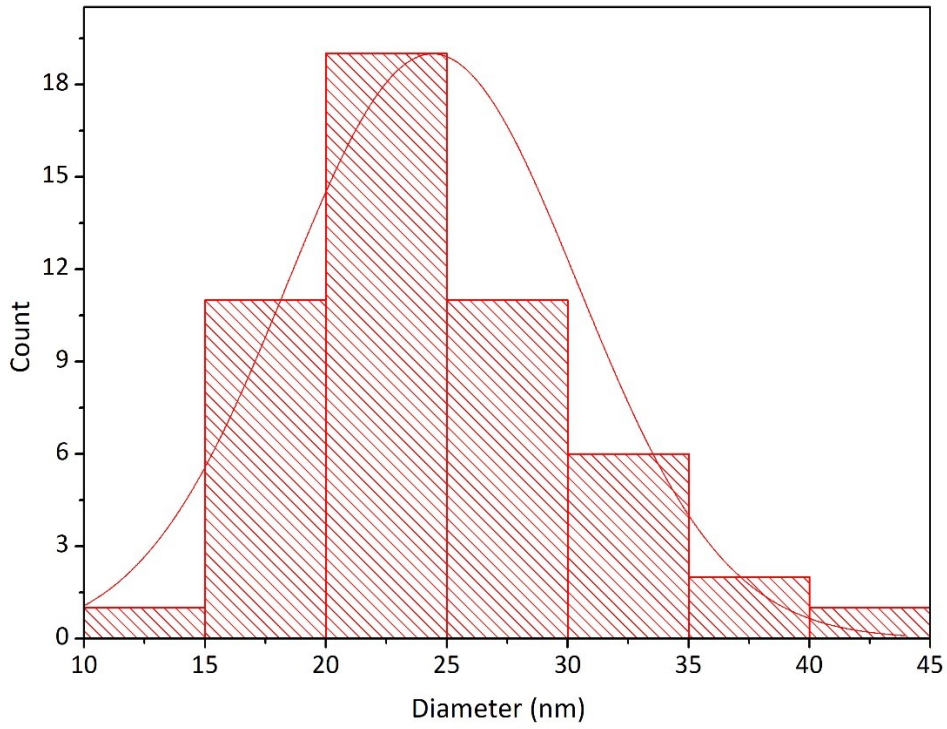

Figure S33. Particle size distribution in the case of **L3** stabilized silver nanoparticles after the addition of Hg^{2+} ions

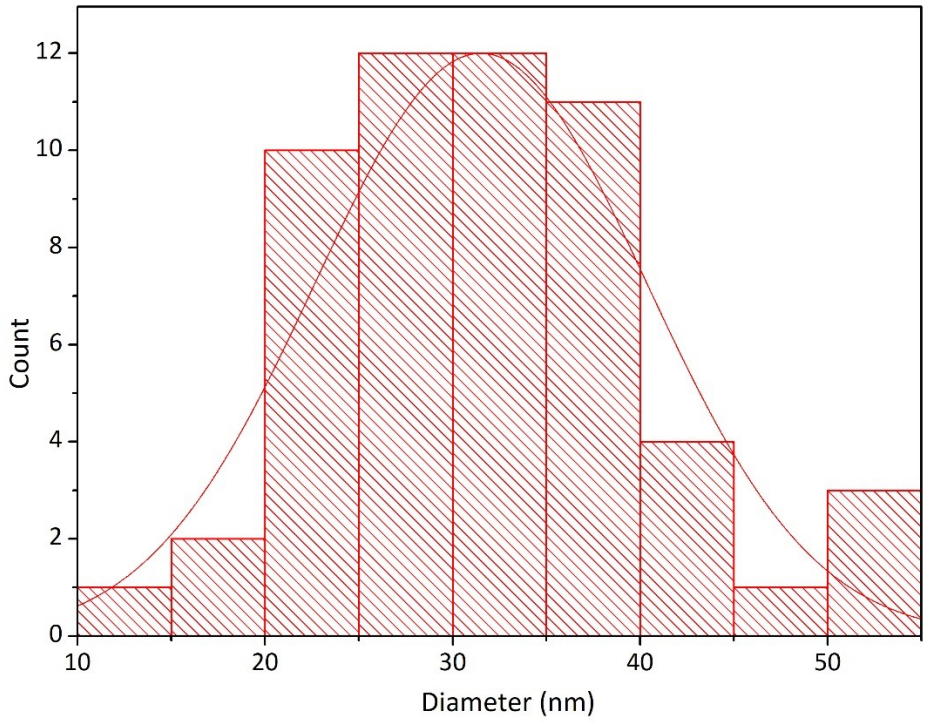

Figure S34. Particle size distribution in the case of **L3** stabilized silver nanoparticles after the addition of HSO_4^- ions

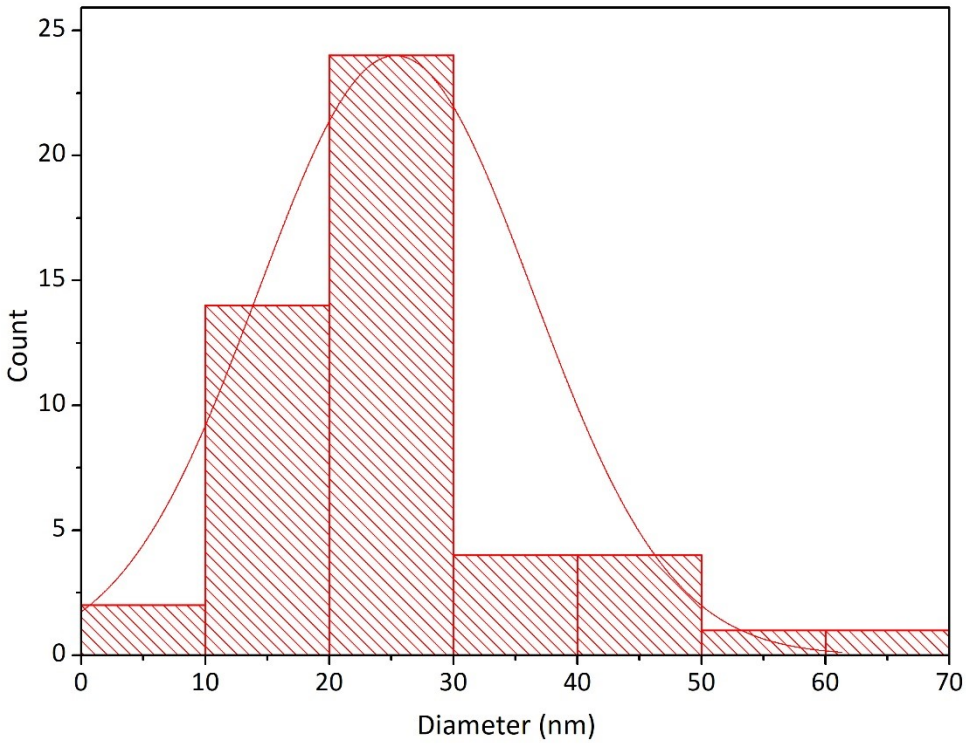

Figure S35. Particle size distribution in the case of **L4** stabilized silver nanoparticles after the addition of Hg^{2+} ions

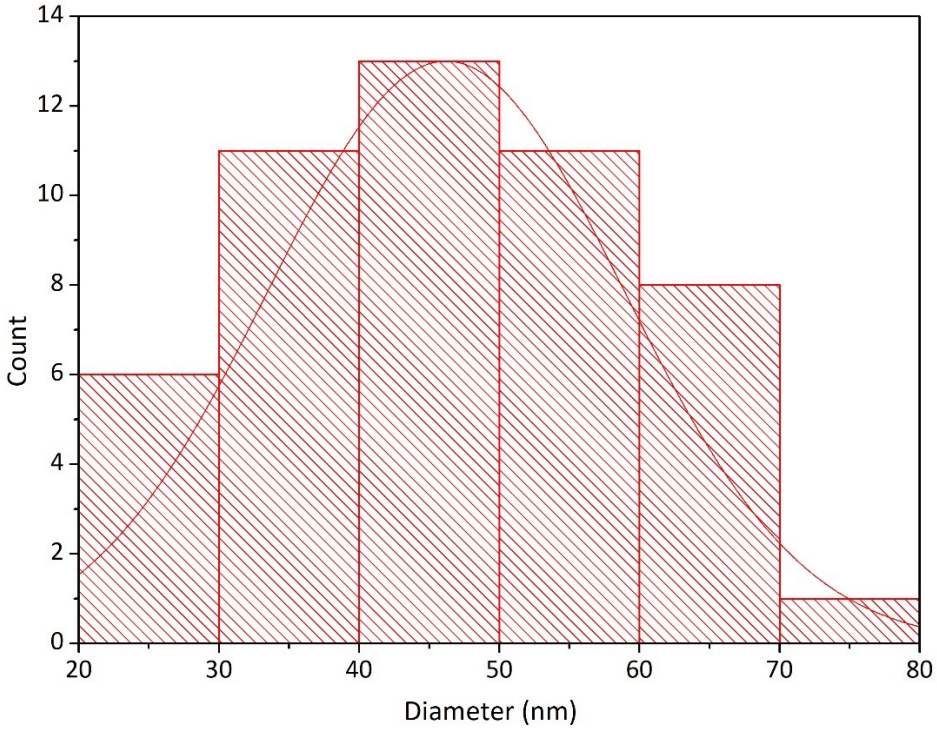

Figure S36. Particle size distribution in the case of **L4** stabilized silver nanoparticles after the addition of Cr^{3+} ions

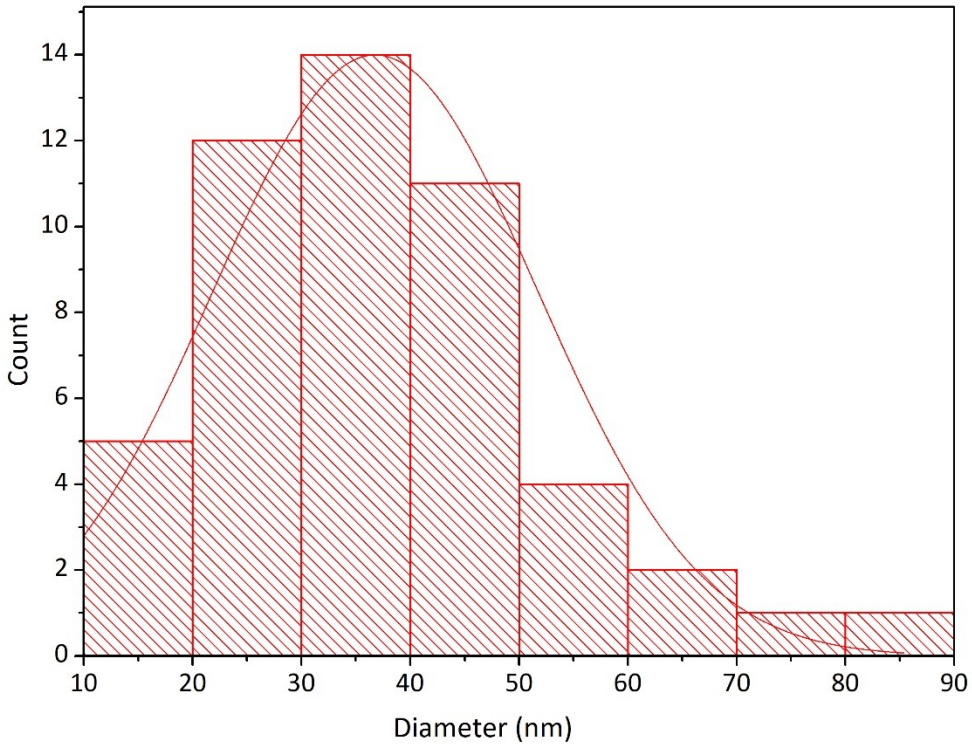

Figure S37. Particle size distribution in the case of **L4** stabilized silver nanoparticles after the addition of Bi^{3+} ions

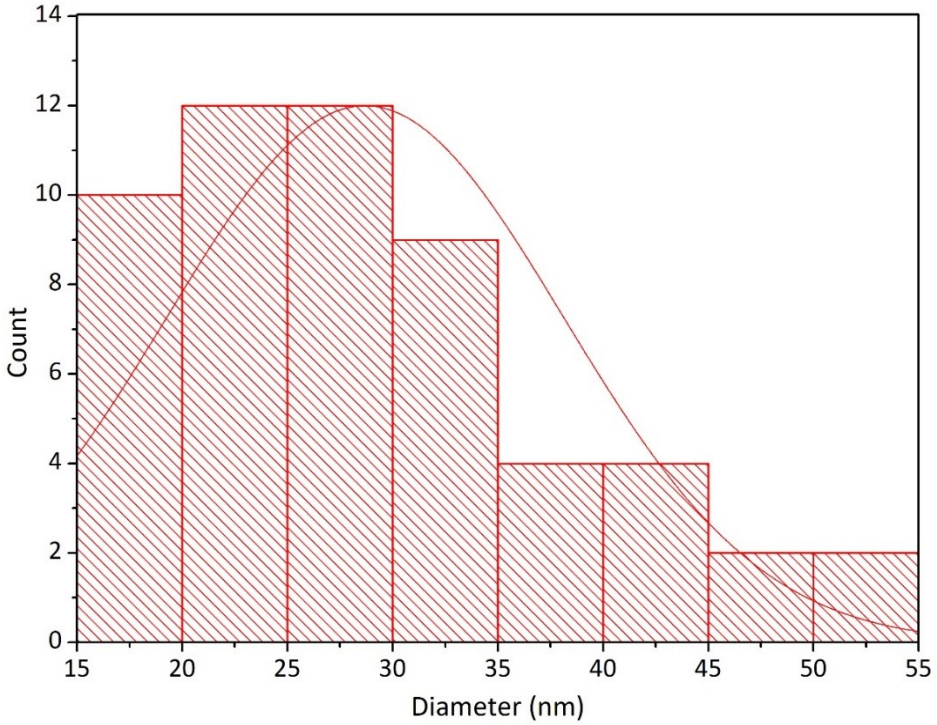

Figure S38. Particle size distribution in the case of **L4** stabilized silver nanoparticles after the addition of HSO_4^- ions

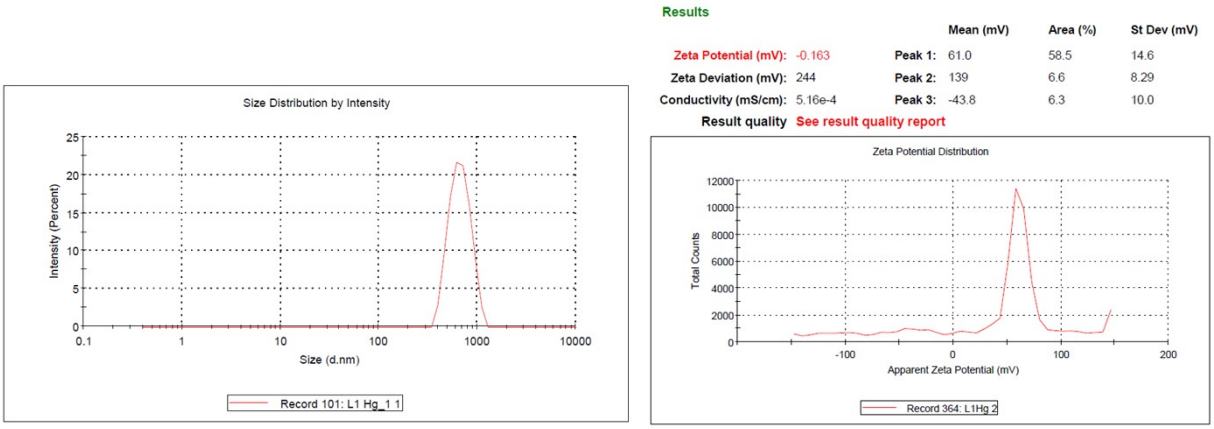

Figure S39. DLS data and zeta potential in the case of **L1** stabilized silver nanoparticles after the addition of Hg^{2+} ions

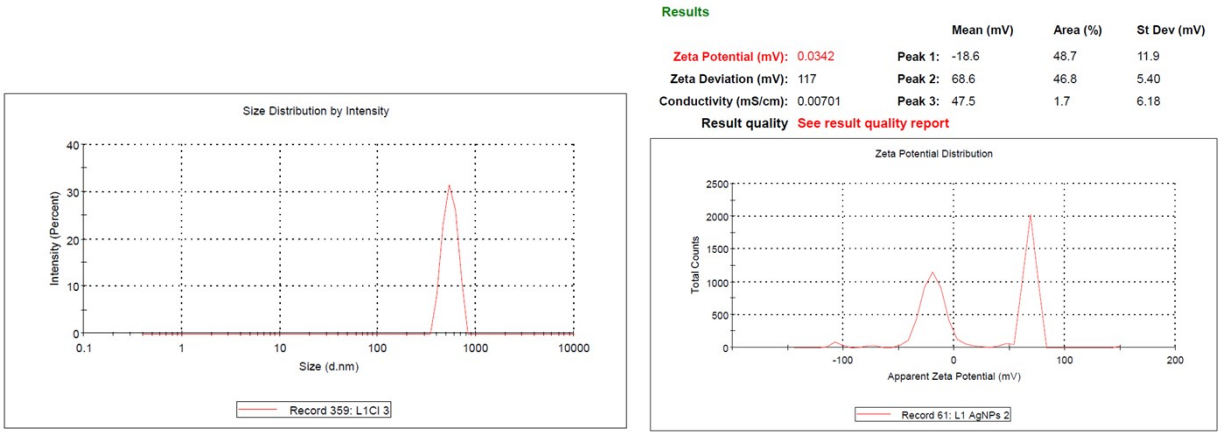

Figure S40. DLS data and zeta potential in the case of **L1** stabilized silver nanoparticles after the addition of Cl^{-} ions

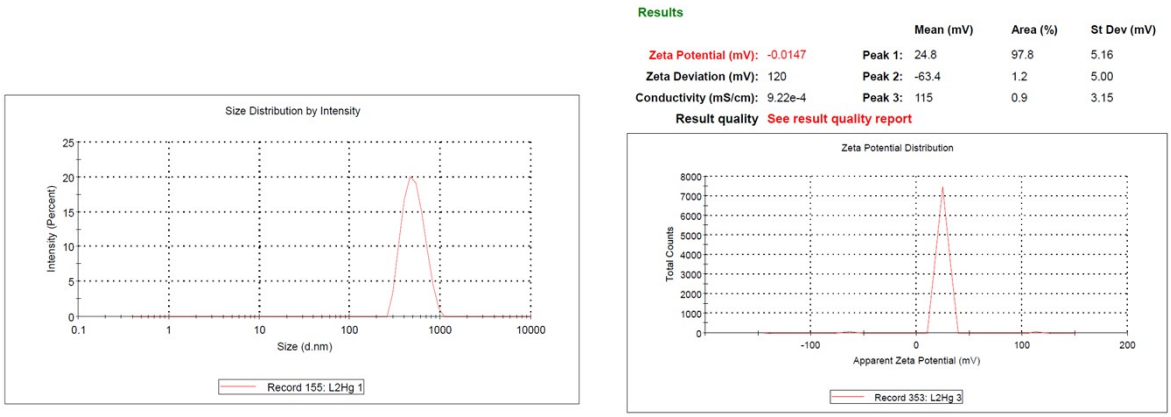

Figure S41. DLS data and zeta potential in the case of **L2** stabilized silver nanoparticles after the addition of Hg^{2+} ions

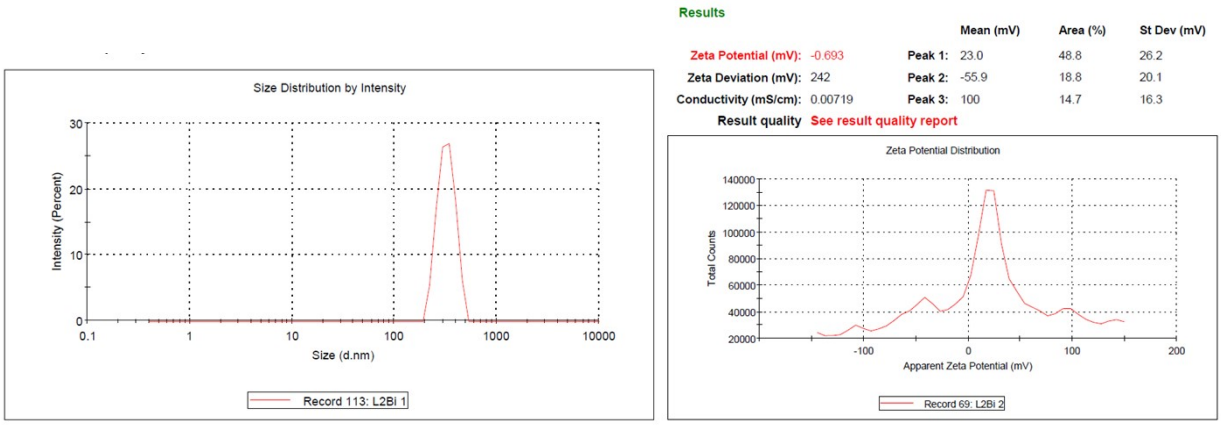

Figure S42. DLS data and zeta potential in the case of **L2** stabilized silver nanoparticles after the addition of Bi^{3+} ions

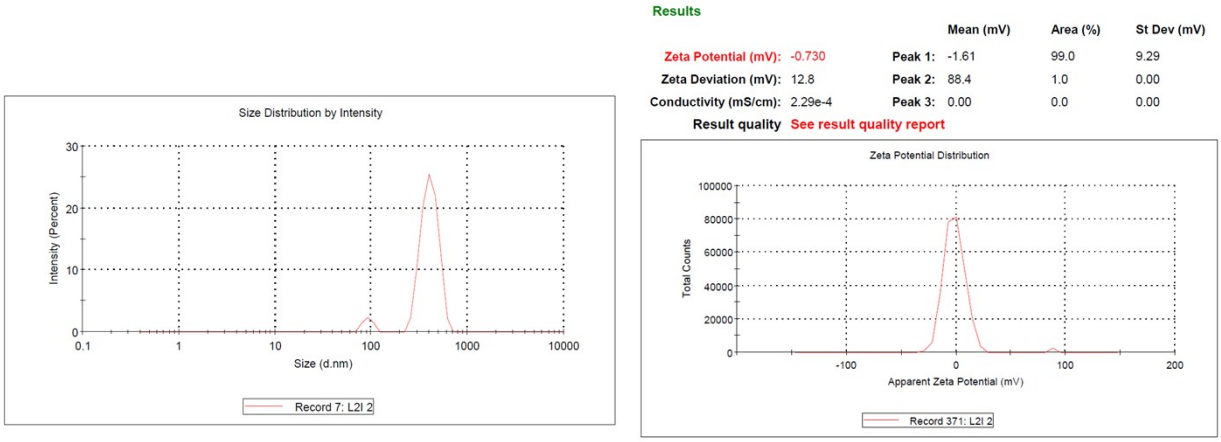

Figure S43. DLS data and zeta potential in the case of **L2** stabilized silver nanoparticles after the addition of I^{-} ions

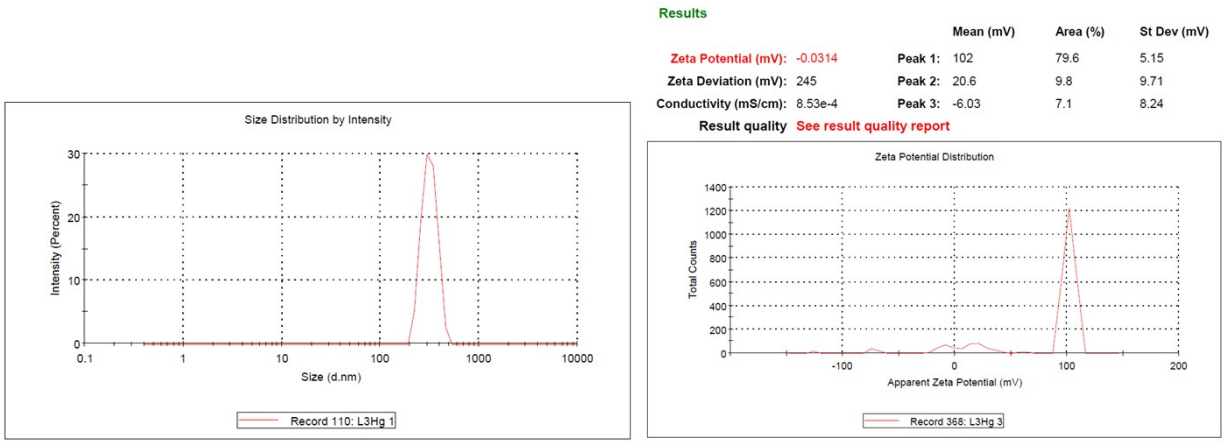

Figure S44. DLS data and zeta potential in the case of **L3** stabilized silver nanoparticles after the addition of Hg^{2+} ions

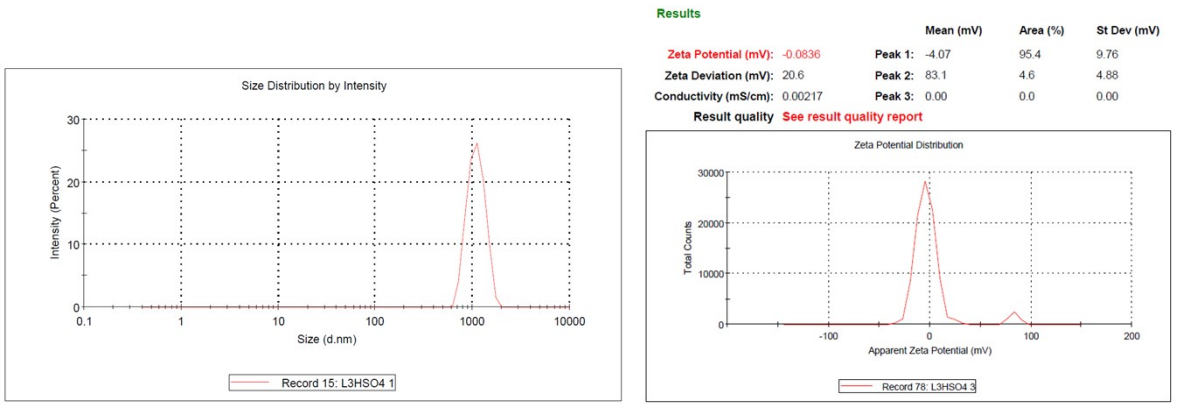

Figure S45. DLS data and zeta potential in the case of **L3** stabilized silver nanoparticles after the addition of HSO_4^- ions

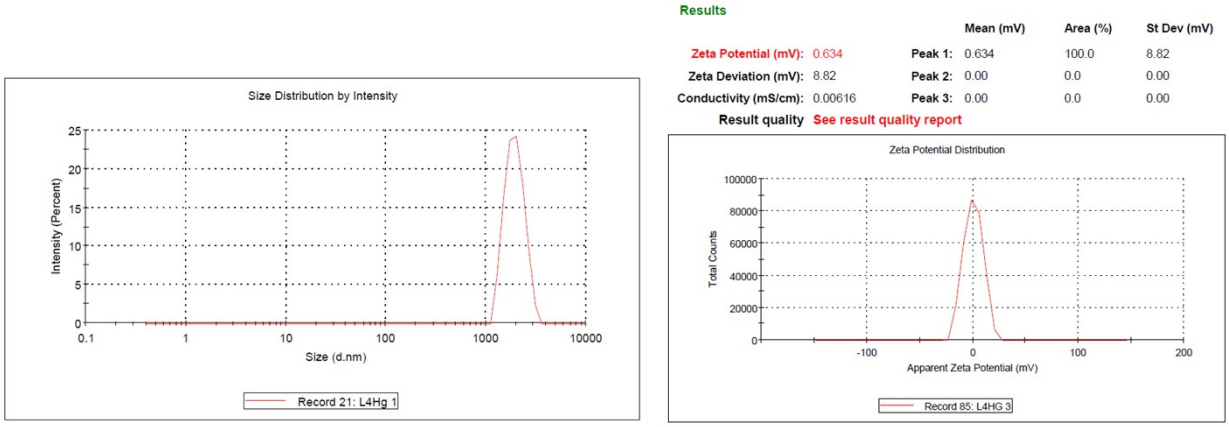

Figure S46. DLS data and zeta potential in the case of **L4** stabilized silver nanoparticles after the addition of Hg^{2+} ions

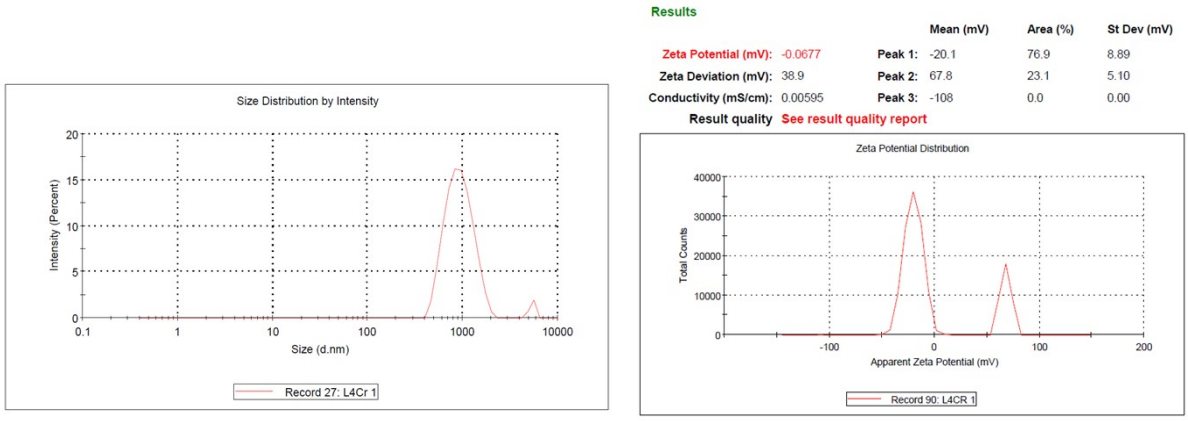

Figure S47. DLS data and zeta potential in the case of **L4** stabilized silver nanoparticles after the addition of Cr^{3+} ions

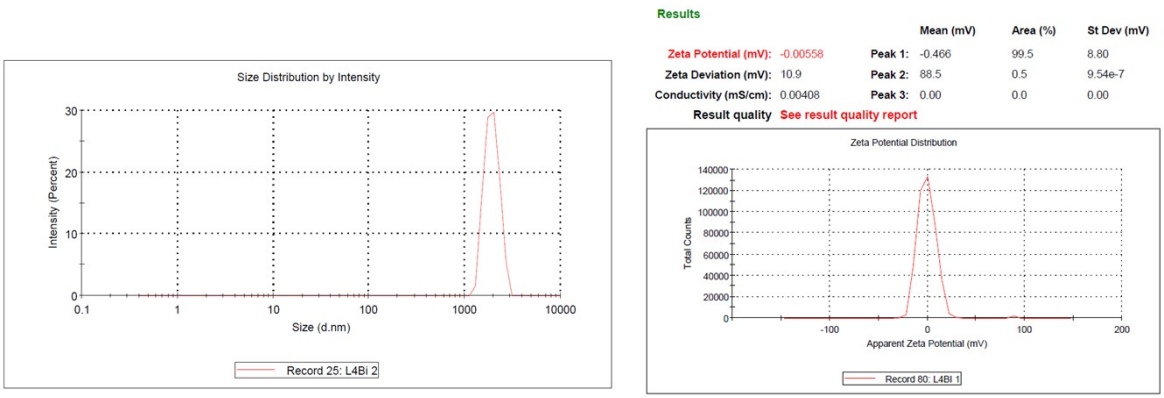

Figure S48. DLS data and zeta potential in the case of **L4** stabilized silver nanoparticles after the addition of Bi^{3+} ions

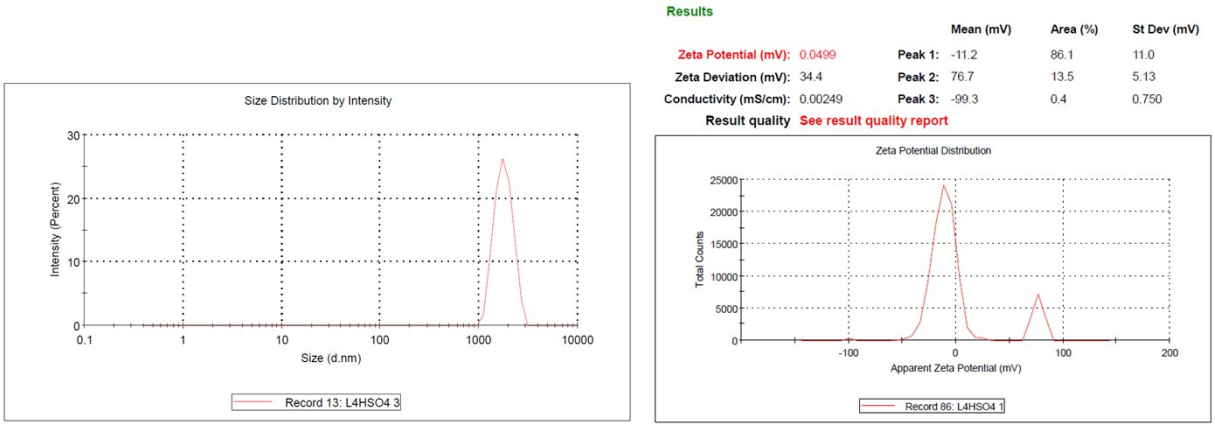

Figure S49. DLS data and zeta potential in the case of **L4** stabilized silver nanoparticles after the addition of HSO_4^- ions

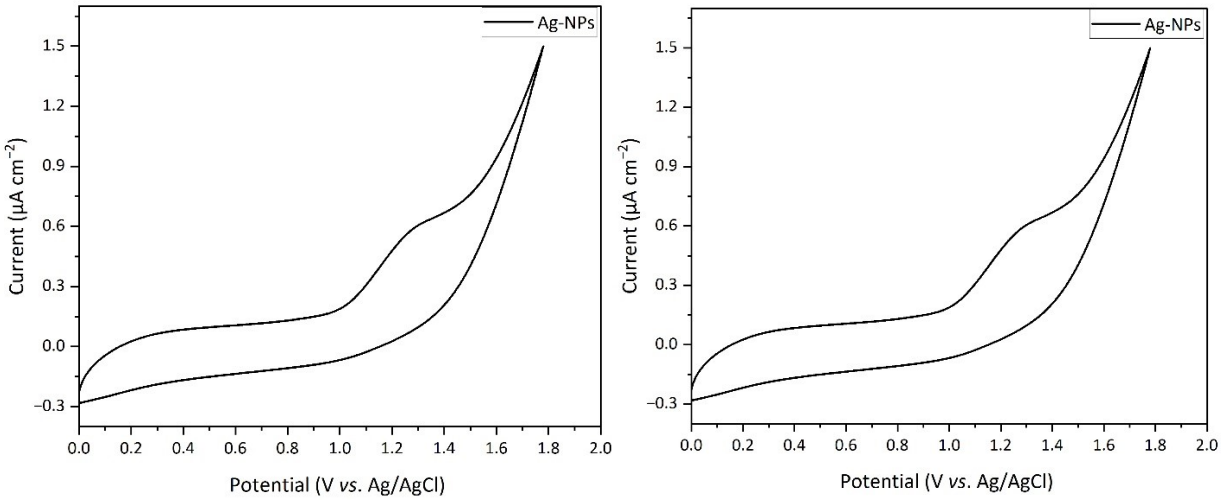

Figure S50. (a) Cyclic voltammogram of **L3** stabilized silver nanoparticles; (b) Differential pulse voltammogram of **L3** stabilized silver nanoparticles and with the addition of I^- ions

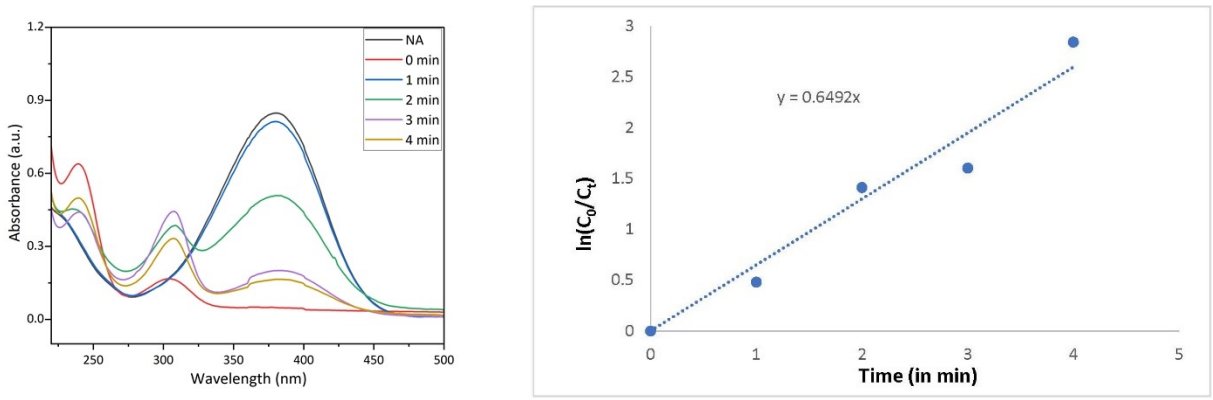

Figure S51. UV spectra of reduction of Nitroaniline and rate constant lnC_0/C_t Vs time

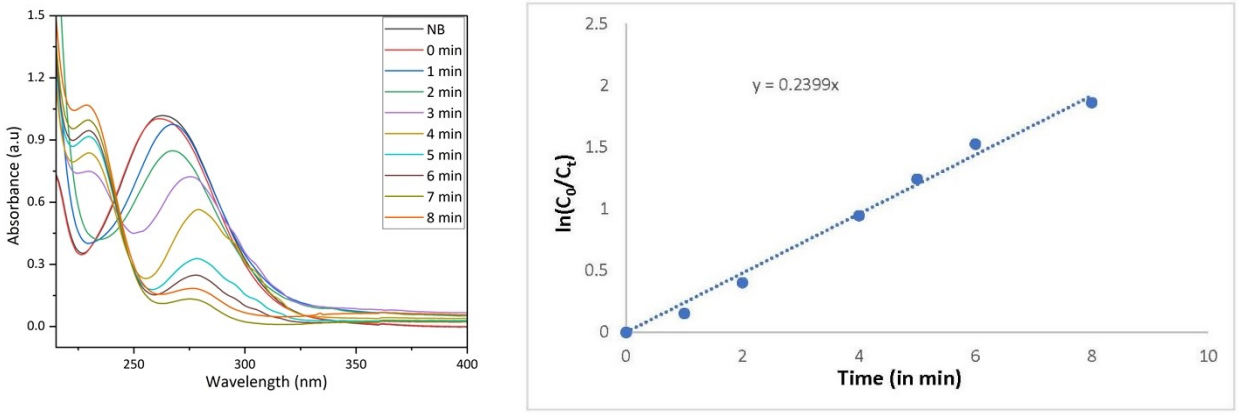

Figure S52. UV spectra of reduction of Nitrobenzene and rate constant lnC_0/C_t Vs time

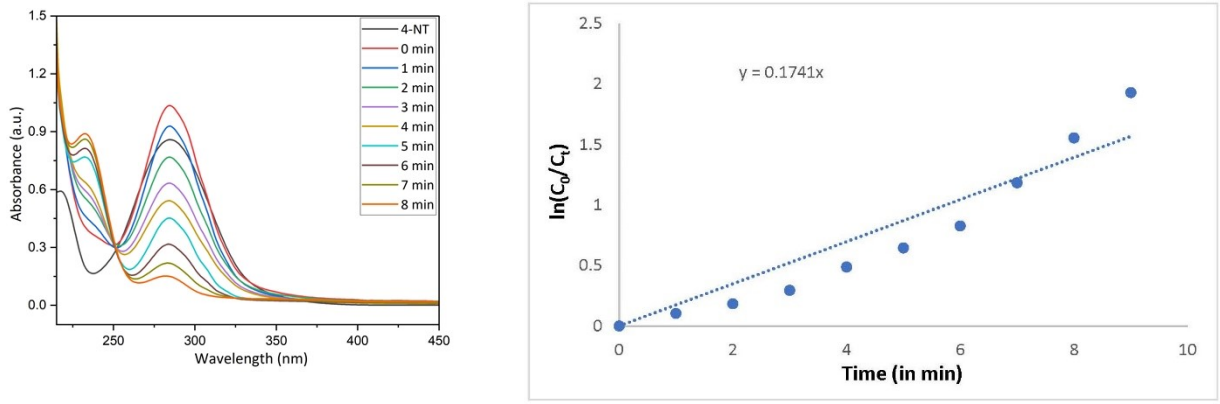

Figure S53. UV spectra of reduction of 4-Nitrotoulene and rate constant lnC_0/C_t Vs time

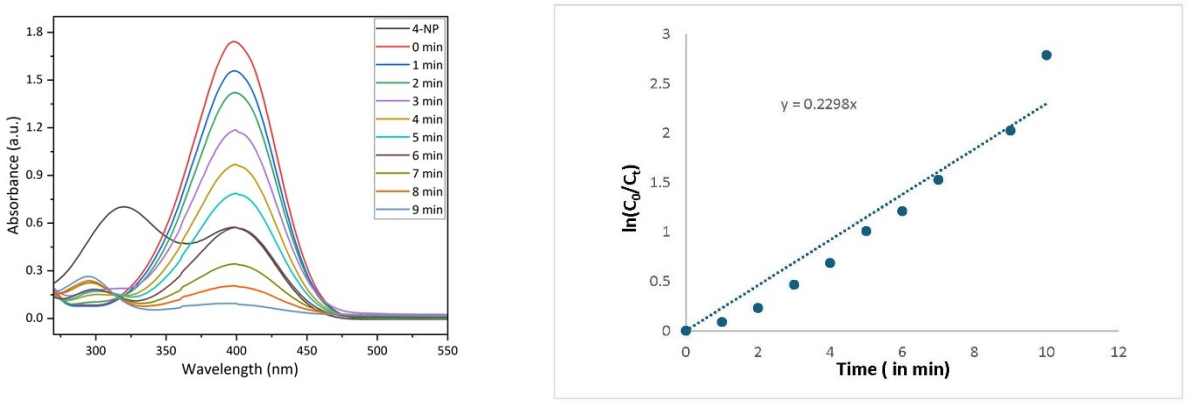

Figure S54. UV spectra of reduction of 4-Nitrophenol and rate constant $\ln C_0/C_t$ Vs time

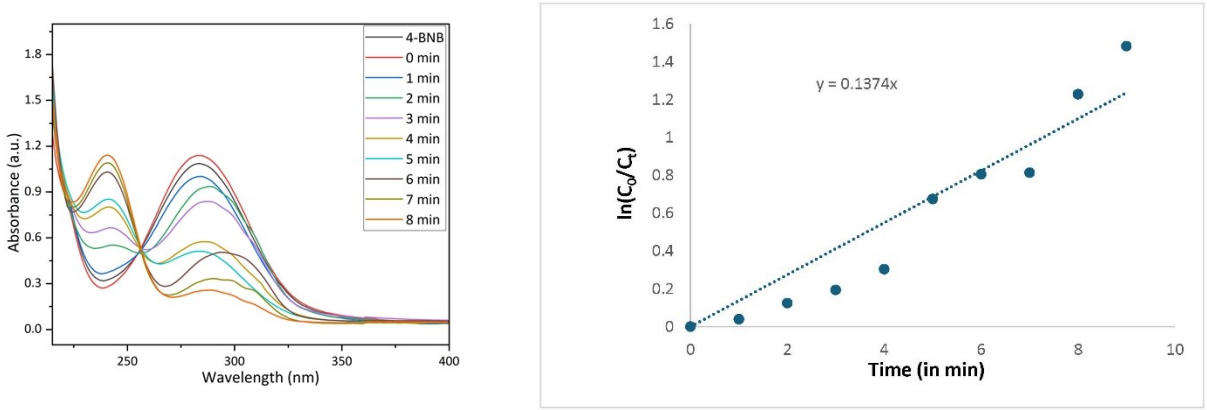

Figure S55. UV spectra of reduction of 1-bromo-4-nitrobenzene and rate constant $\ln C_0/C_t$ Vs time

Results

		Mean (mV)	Area (%)	St Dev (mV)
Zeta Potential (mV): -26.1	**Peak 1:**	-26.1	100.0	5.64
Zeta Deviation (mV): 5.64	**Peak 2:**	0.00	0.0	0.00
Conductivity (mS/cm): 0.0121	**Peak 3:**	0.00	0.0	0.00
Result quality Good				

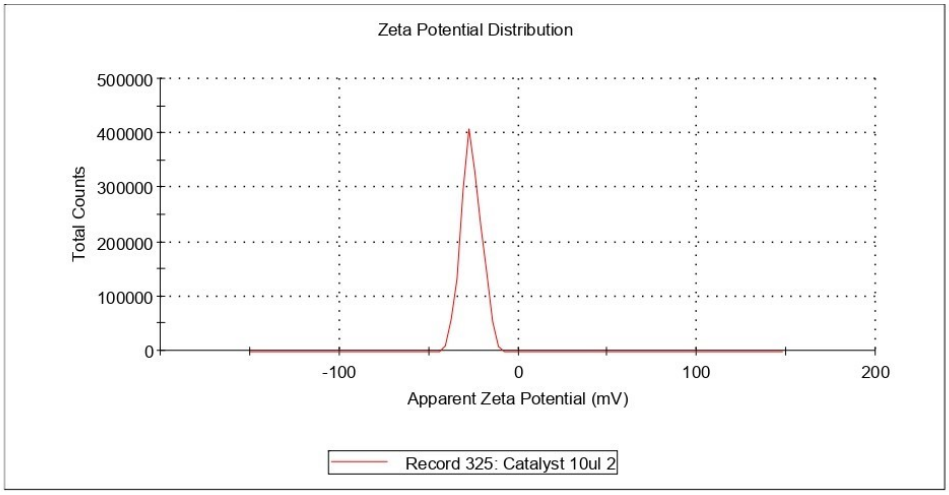

Figure S56. Surface charge on the catalyst

Results

		Mean (mV)	Area (%)	St Dev (mV)
Zeta Potential (mV): -43.5	**Peak 1:**	-43.5	100.0	10.2
Zeta Deviation (mV): 10.2	**Peak 2:**	0.00	0.0	0.00
Conductivity (mS/cm): 0.329	**Peak 3:**	0.00	0.0	0.00
Result quality Good				

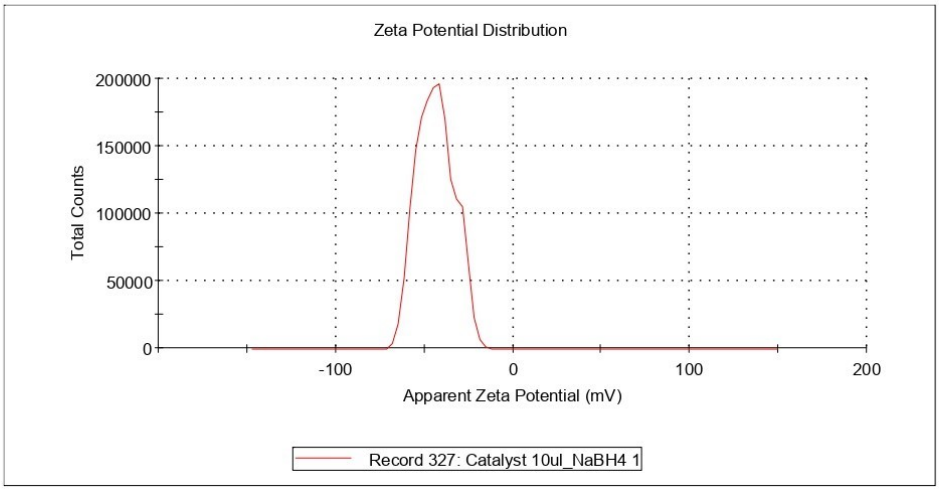

Figure S57. Surface charge after the addition of $NaBH_4$ and 4-nitrophenol in the catalyst solution

Results

		Mean (mV)	Area (%)	St Dev (mV)
Zeta Potential (mV): -28.2	**Peak 1:**	-28.2	100.0	6.29
Zeta Deviation (mV): 6.29	**Peak 2:**	0.00	0.0	0.00
Conductivity (mS/cm): 0.206	**Peak 3:**	0.00	0.0	0.00
Result quality Good				

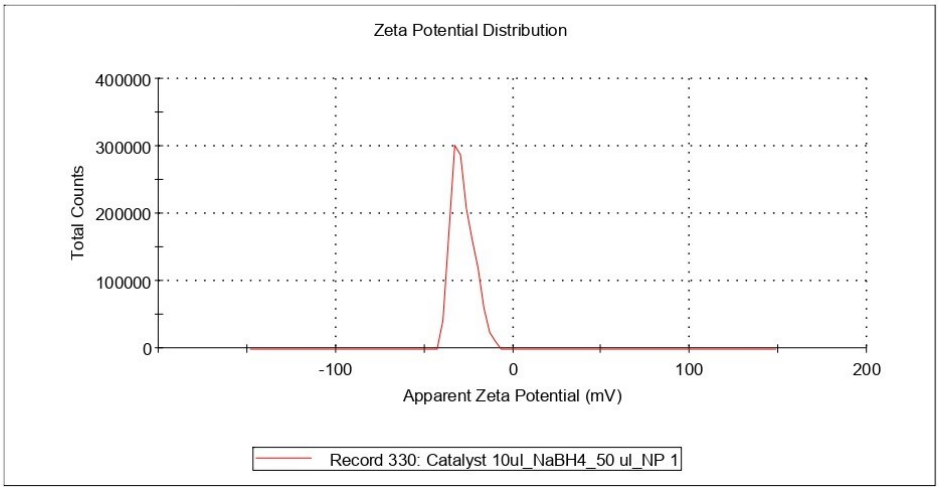

Figure S58. Surface charge after completion of reaction

Table S1. Ag-NPs synthesized using imine containing small molecules for various applications

S. No.	Metal precursor and reducing agent	Imine containing small molecule	Size of NPs	Application	Reference
1.	$AgNO_3$, $NaBH_4$	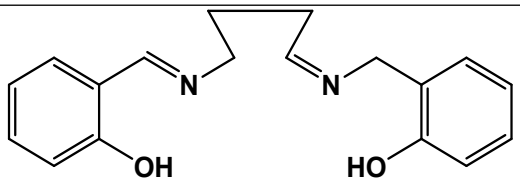	29.93 nm	Detection of toxic metal (Hg^{2+}) and catalytic application of dye degradation.	1
2.	$AgNO_3$, $NaBH_4$	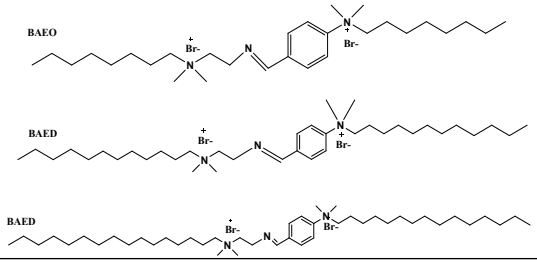	10 ± 25 nm	Catalyst to reduce nitroaromatic compounds	2
3.	$AgNO_3$, $NaBH_4$	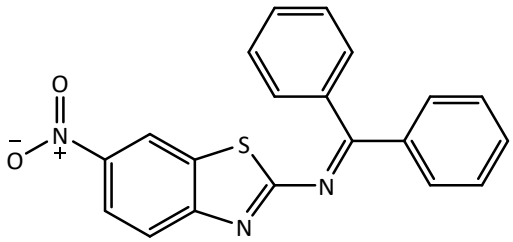	72 nm	Good antibacterial activity against pathogenic propionic bacteria with comparative studies	3
4.	$AgNO_3$, Hydrazine	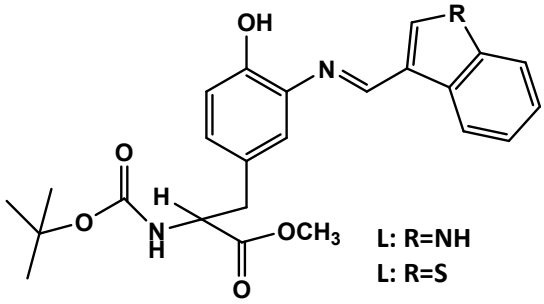	12 ± 3.5 nm	Detection of Cu^{2+} ions in the absolute ethanol solution	4

5.	$AgNO_3$, $NaBH_4$	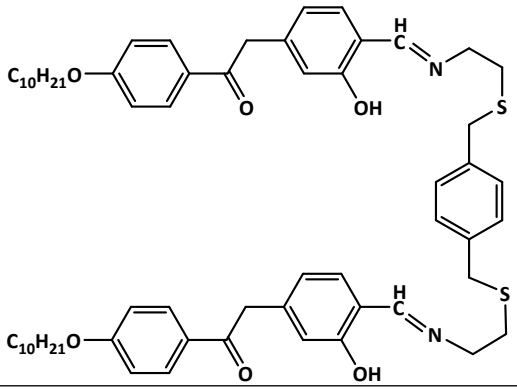	5 nm	Colorimetric detection of Hg^{2+} and Cu^{2+} ions and catalytic reduction of nitroaromatics.	5

References:

1. A. Minhaz, N. Khan and N. Jamila, *Arab J. Chem.*, 2020, **13**, 8898–8908.
2. E. Badr, S. Shafek, H. Hefni, A. Elsharif, A. Alanezi, S. Shaban and D. Kim*, J. Mol. Liq.*, 2021, **326**, 115342.
3. K. Kumar, S. Anand, M. Kori, N. Mishra and S.P. Shrivastava, *J. Indian Chem Soc.*, 2023, **100**, 100965.
4. E. Oliveira, J. Miranda and H. Santos, *Inorganica Chim Acta.*, 2012, **380**, 22-30.
5. N. Yadav, S. Shiva, P. Oswal, A. Kumar, A.K. Singh, B. Singh, B. Pandit, J. Ahmed and G. K. Rao, *J. Mol. Liq.*, 2023, **377**, 121531.